

RESEARCH ARTICLE

Smooth muscle differentiation shapes domain branches during mouse lung development

Katharine Goodwin¹, Sheng Mao², Tristan Guyomar^{2,3}, Erin Miller⁴, Derek C. Radisky⁴, Andrej Košmrlj² and Celeste M. Nelson^{5,6,*}

ABSTRACT

During branching morphogenesis, a simple cluster of cells proliferates and branches to generate an arborized network that facilitates fluid flow. The overall architecture of the mouse lung is established by domain branching, wherein new branches form laterally off the side of an existing branch. The airway epithelium develops concomitantly with a layer of smooth muscle that is derived from the embryonic mesenchyme. Here, we examined the role of smooth muscle differentiation in shaping emerging domain branches. We found that the position and morphology of domain branches are highly stereotyped, as is the pattern of smooth muscle that differentiates around the base of each branch. Perturbing the pattern of smooth muscle differentiation genetically or pharmacologically causes abnormal domain branching. Loss of smooth muscle results in ectopic branching and decreases branch stereotypy. Increased smooth muscle suppresses branch initiation and extension. Computational modeling revealed that epithelial proliferation is insufficient to generate domain branches and that smooth muscle wrapping is required to shape the epithelium into a branch. Our work sheds light on the physical mechanisms of branching morphogenesis in the mouse lung.

KEY WORDS: Mechanical stress, Symmetry breaking, Tissue morphodynamics

INTRODUCTION

Branching morphogenesis begins with a simple tube or cluster of cells that grows and undergoes rounds of budding and/or bifurcation, leading to the formation of a complex, arborized network. The final form and function of each branched organ varies, but the molecular programs responsible for their development are often similar. In most branched epithelial tissues, growth factors from the surrounding mesenchyme signal to the epithelium to elicit cellular behaviors required for growth and branching (Wang et al., 2017). However, growth factor signaling alone cannot fully explain how the different architecture of each organ is achieved. To understand how branched networks are generated, we require a deeper understanding of the physical mechanisms of branching morphogenesis (Varner and


Nelson, 2014). Equipped with such knowledge, we may be able to diagnose and treat developmental disorders more effectively, and further, to reproduce the mechanisms employed by the embryo to engineer branched tissues *ex vivo*.

The branching pattern of the mouse airway epithelium is highly stereotyped; the same sequence of branching events occurs in every embryo (Metzger et al., 2008). Each branching event can be categorized as either terminal bifurcation or domain branching. Bifurcation splits the tip of a branch into two daughter branches, whereas domain branching generates new buds off the side of an existing parent branch. The exact cellular mechanisms required for domain branching in the mouse lung are still being elucidated. In the chicken lung, domain branches are initiated through apical constriction of the airway epithelium; initially columnar cells assume a trapezoidal morphology as their apical domains narrow, causing the tissue to bend outwards into the surrounding mesenchyme (Kim et al., 2013). Although trapezoid-shaped cells have been reported in the murine lung (Kadzic et al., 2014), it remains unclear whether apical constriction physically drives the process of domain branching or whether cells become trapezoidal as a result of changes in tissue topology associated with branch formation. Patterned proliferation has long been proposed to drive branching morphogenesis, but has never been directly tied to branch initiation (Ettensohn, 1985; Varner and Nelson, 2014). After branches initiate in the mouse lung, higher proliferation rates are observed in the epithelial cells within the emerging branch than in the neighboring non-branching epithelium (Schnatwinkel and Niswander, 2013). Finally, physical instabilities generated by constrained growth of the epithelium have been shown to induce buckling in mesenchyme-free culture (Varner et al., 2015); differences in the relative proliferation rates of the epithelium and mesenchyme of the lung might serve a similar role for initiating branches *in vivo*.

The mesenchyme of the embryonic lung provides both molecular and physical signals that guide branching of the airway epithelium. Smooth muscle cells that encircle the airways are derived from mesenchymal progenitors that relocate around the epithelium as it extends distally. Fibroblast growth factor 9 (FGF9) secreted by the mesothelium surrounding the lungs maintains the progenitor status of mesenchymal cells (Weaver et al., 2003; Yi et al., 2009). Blocking FGF9 signaling by knocking out *Fgfr1* and *Fgfr2* in the pulmonary mesenchyme results in ectopic smooth muscle differentiation and reduced epithelial branching (Yi et al., 2009). The exact identity of smooth muscle progenitors is unclear; FGF10- and Wilms tumor 1 (WT1)-expressing progenitors give rise to a minor fraction of smooth muscle cells at embryonic day (E)15.5 and E18.5, whereas glioma-associated oncogene 1 (Gli1)- and Axin2-expressing progenitors give rise to the majority of smooth muscle cells at E18.5 (Moiseenko et al., 2017). However, Gli1⁺ and Axin2⁺ cells are found throughout the lung and are not restricted to the smooth muscle lineage (Moiseenko et al., 2017).

¹Lewis-Sigler Institute for Integrative Genomics, Princeton University, Princeton, NJ 08544, USA. ²Department of Mechanical and Aerospace Engineering, Princeton University, Princeton, NJ 08544, USA. ³Département de Physique, Ecole Normale Supérieure de Lyon, F-69342 Lyon, France. ⁴Department of Cancer Biology, Mayo Clinic Cancer Center, Jacksonville, FL 32224, USA. ⁵Department of Chemical and Biological Engineering, Princeton University, Princeton, NJ 08544, USA. ⁶Department of Molecular Biology, Princeton University, Princeton, NJ 08544, USA.

*Author for correspondence (celesten@princeton.edu)

 C.M.N., 0000-0001-9973-8870

Epithelial branching is regulated by reciprocal signaling between the mesenchyme and the epithelium. FGF10 produced by the mesenchyme signals to the epithelium to increase proliferation and to induce Sonic hedgehog (Shh) expression, which in turn inhibits FGF10 expression (Herriges et al., 2015; Menshykau et al., 2012). This signaling loop is required for branching morphogenesis, but the physical mechanisms by which FGF10 and Shh expression lead to changes in epithelial geometry are still unclear. Recent studies point to a role for smooth muscle differentiation in epithelial branching (Jaslove and Nelson, 2018). In particular, we found that patterned smooth muscle differentiation is required for bifurcation of the airway epithelium (Kim et al., 2015). Prior to bifurcation, smooth muscle differentiates at the tip of the epithelial bud, specifying the future cleft site. As more smooth muscle differentiates it splits the bud in half, thus inducing bifurcation. Blocking or enhancing smooth muscle differentiation prevents normal cleft specification and epithelial bifurcation (Kim et al., 2015). Components of the signaling loop known to be important for epithelial branching also regulate smooth muscle differentiation. Shh induces mesenchymal precursors to differentiate into smooth muscle, and deletion of Shh in the airway epithelium prevents smooth muscle differentiation and leads to severely hypoplastic lungs (Miller et al., 2004; Pepicelli et al., 1998). *Fgf10* hypomorphic embryos have decreased airway smooth muscle, although this may be an indirect effect due to reduced Shh expression in the epithelium (Ramasamy et al., 2007). Taken together, these findings suggest that FGF10-induced Shh expression and secretion by epithelial tip cells could lead to local smooth muscle differentiation, cleft specification, and bifurcation.

Whether smooth muscle differentiation is also involved in domain branching remains unknown. Airway smooth muscle is present at the earliest stages of lung development when domain branches first form and is detected initially around the proximal airways and elaborated distally over the course of branching morphogenesis. Domain branches form in a proximal-to-distal order and are accompanied by recruitment of smooth muscle; it is possible that the local differentiation of smooth muscle controls or influences the initiation of domain branches similar to the way it specifies epithelial clefting during bifurcation. Here, we investigated whether smooth muscle plays a role in domain branching of the murine lung. We found that domain branches are formed through conserved changes in morphology: wide emerging buds thin at their bases as they extend. Simultaneously, smooth muscle wrapping increases around the primary bronchus on either side of the growing bud. Disrupting smooth muscle differentiation in cultured lung explants leads to abnormal domain branching. Increased smooth muscle differentiation suppresses branch initiation and extension, whereas decreased differentiation leads to ectopic branching and alterations in branch positioning. Using a combination of experimental and modeling approaches, we evaluated the roles of epithelial proliferation and smooth muscle-mediated constraints in emerging domain branches. We found that manipulating smooth muscle wrapping has mild and likely indirect effects on local patterns of proliferation in the parent branch, and that proliferation alone cannot generate domain branches correctly. Instead, smooth muscle-mediated constraint and constriction control parent branch morphology during domain branching. These data suggest that smooth muscle is required for sculpting both bifurcations and domain branches in the embryonic mouse lung. Based on these findings, we propose that the propensity of the epithelium to grow and branch in response to growth factors from the mesenchyme is restricted by spatially patterned smooth muscle in order to achieve the final branching pattern.

RESULTS

Domain branches and smooth muscle sheath form stereotypically and concomitantly in the embryonic mouse lung

During murine lung development, domain branching generates the overall architecture of the airway epithelium (Metzger et al., 2008). From E11.5 to E12.5, domain branches extend laterally off the left and right caudal lobes. We focused on understanding the potential role of airway smooth muscle in development of the second domain branch, hereafter referred to as L.L2, as well as the first domain branch of the right caudal lobe, RCd.L1, which are representative of the other domain branches in the lung. The first branch of the left lobe, L.L1, forms at a stage of development less amenable to study in cultured explants; further, L.L1 is the only domain branch that is flanked proximally by both smooth muscle and cartilage each wrapped halfway around the primary bronchus, and was therefore excluded from our analysis (Miller et al., 2004).

In lungs dissected from embryos at E12, we found that domain branches form consistently in precise positions along the left primary bronchus (Fig. 1A,B). Further, time-lapse imaging of lungs explanted at E11.5 and cultured for 24 h revealed that the morphology of the domain branch evolves in a stereotyped manner, with the width of the base of the branch decreasing as the branch elongates (Fig. 1C,D, Movie 1). We mapped smooth muscle coverage around the emerging branch using lungs from E11.5 to E12.5. To visualize smooth muscle localization, we reconstructed cross-sections through confocal z-stacks of the airway epithelium in lungs immunostained for E-cadherin (Ecad; also known as cadherin 1) and α -smooth muscle actin (α SMA; ACTA2). Smooth muscle recruitment was quantified by measuring α SMA staining intensity around the circumference of the airway and plotting intensity as a function of angle with respect to the center of the bronchus. At E12, proximal to L.L1 (region C1), smooth muscle is localized to the medial half of the bronchus (Fig. 1E-G), and cartilage surrounds the lateral side (Miller et al., 2004). At the level of each domain branch (regions C2 and C4) smooth muscle is restricted to the medial side of the bronchus as the epithelium extends laterally (Fig. 1E-G). Between domain branches and distal to branch L.L2, smooth muscle wraps the entire circumference of the primary bronchus (regions C3 and C5; Fig. 1E-G). We observed similar patterns in the right caudal lobe: the first domain branch of this lobe (RCd.L1) forms at a consistent and stereotyped position, thins as it elongates, and is surrounded by a pattern of smooth muscle identical to that observed around L.L2 (Fig. S1A-D). Additionally, α SMA-expressing cells wrapped around the airways were also positive for EGFP expression directed by the smooth muscle myosin heavy chain (*Myh11*) promoter, consistent with airway smooth muscle differentiation (Fig. S2A).

To determine whether changes in branch morphology are accompanied by changes in smooth muscle coverage, we examined lungs from embryos at different developmental stages. We found that as domain branches elongate and thin from E11.5 to E12.5, smooth muscle coverage around the primary bronchus increases (Fig. 1H-J, Fig. S3). These data suggest that domain branching of the epithelium and spatial patterns of smooth muscle differentiation are correlated during early development of the mouse lung.

Perturbation of smooth muscle differentiation disrupts patterned smooth muscle coverage

To determine whether the pattern of smooth muscle around the airways is important for domain branching, we pharmacologically disrupted smooth muscle differentiation in lungs explanted at E11.5

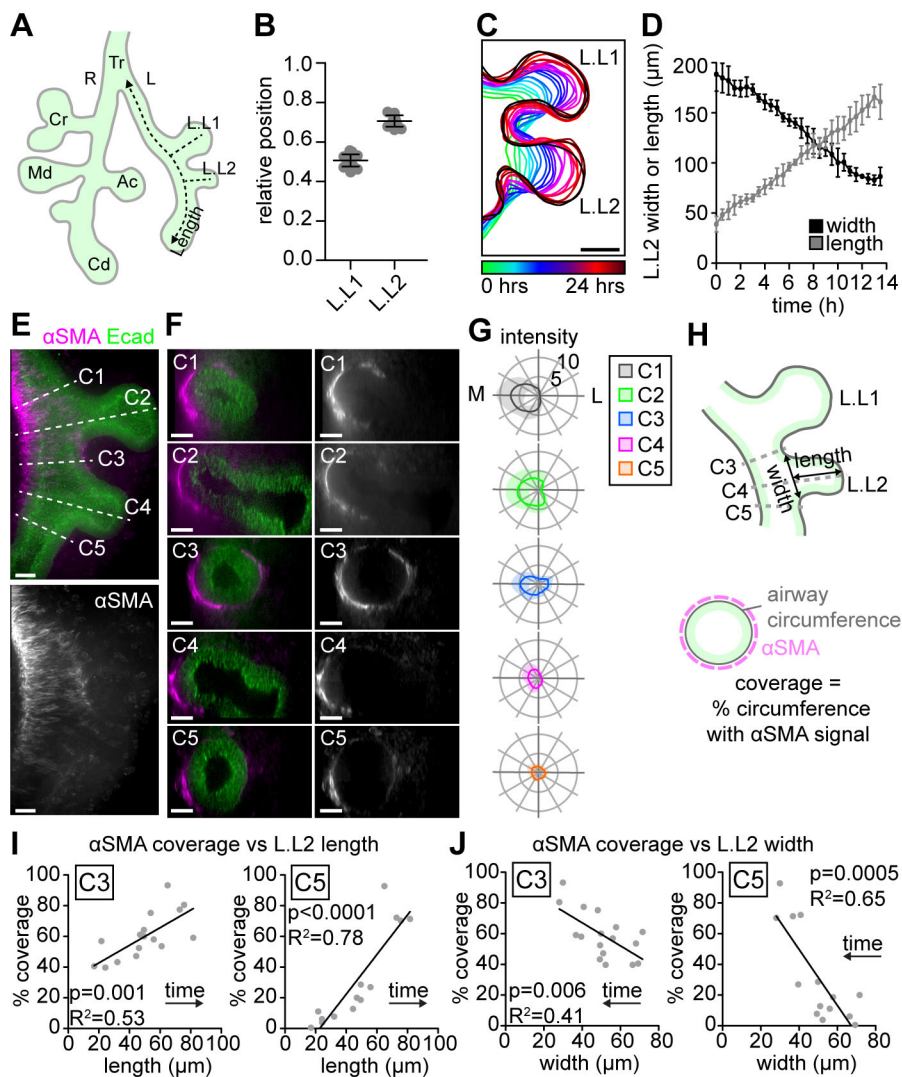


Fig. 1. Domain branches and airway smooth muscle develop stereotypically. (A) Schematic of E12 CD1 mouse lung indicating the trachea (Tr), right lobes (R: Cr, Md, Ac, Cd), left lobe (L), and domain branches (L.L1 and L.L2). (B) Relative positions of domain branches L.L1 and L.L2 in E12 lungs measured as distance from the tracheal fork divided by length of the left bronchus ($n=19$). Error bars indicate s.d. (C) Contours of domain branches L.L1 and L.L2 during 24 h time-lapse imaging. Contours are 1 h apart. Scale bar: 25 μ m. (D) Width and length of L.L2 over the course of 24 h time-lapse imaging ($n=4$). Error bars indicate s.d. (E, F) Single z-slices (E) and reconstructed cross-sections (F) of the left lobe of an E12 lung immunostained for E-cadherin (Ecad) and α SMA. Cross-sections are from locations C1-C5 as indicated in E. Scale bars: 25 μ m. (G) Polar plots showing mean total α SMA intensity relative to background intensity around the airway based on angle from the center of the bronchus ($n=11$). Dark lines show the mean and shaded regions show s.d. (H) Schematics showing branch width, length and locations of cross-sections C3-C5 (top) and airway circumference and smooth muscle coverage (bottom). (I, J) Smooth muscle coverage versus length (I) or width (J) at the level of C3 and C5 ($n=15-17$). Results of linear regression including P -value and R^2 values are indicated on each plot.

and cultured for 24 h. We inhibited smooth muscle differentiation by treating explants with nifedipine or cyclopamine. Nifedipine is an L-type calcium channel blocker that specifically prevents smooth muscle contraction (McCray, 1993; Roman, 1995) and differentiation (Kim et al., 2015). Explants treated with nifedipine exhibited reduced smooth muscle wrapping around the primary bronchus near emerging domain branches (Fig. 2, Figs S1E and S4A). Cyclopamine is a Shh antagonist and thus prevents differentiation of mesenchymal cells into airway smooth muscle (Chen et al., 2002a). In explants treated with cyclopamine, smooth muscle wrapping around the bronchus near domain branches was almost completely eliminated (Fig. 2, Figs S1E and S4A).

Conversely, we increased smooth muscle coverage around emerging domain branches by treating explants with SU5402 or smoothed agonist (SAG). SU5402 is a fibroblast growth factor receptor 1 (FGFR1) tyrosine kinase inhibitor that blocks the FGF signaling to the mesenchyme required to maintain mesenchymal state and prevent differentiation into smooth muscle (Mohammadi et al., 1997; Yi et al., 2009). SAG activates Shh signaling and leads to increased smooth muscle differentiation around the airways flanking domain branches (Chen et al., 2002b; Radzikinas et al., 2011). Increasing smooth muscle differentiation with SU5402 or SAG led to more smooth muscle around the airway (Fig. 2,

Figs S1E and S4A). Taken together, we determined that these four pharmacological treatments, each targeting different aspects of smooth muscle differentiation, could robustly decrease (nifedipine and cyclopamine) or increase (SU5402 and SAG) smooth muscle wrapping around the epithelium.

Using these treatments to manipulate smooth muscle coverage, we were then able to assess the effects of smooth muscle on domain branching. We found that suppressing or enhancing smooth muscle differentiation results in abnormal positioning of domain branches with increased variance in both the left lobe and the right caudal lobe (Figs S1F and S4A-C). These data show that altering smooth muscle coverage compromises the stereotyped positioning of domain branches.

Disruption of smooth muscle localization results in abnormal branch initiation and morphology

Using the above-described pharmacological approaches to provide us with a dynamic view of epithelial branching, we tested whether the pattern of smooth muscle coverage is required for normal branch formation. We found that decreasing smooth muscle wrapping increases the frequency of branch initiation in the left and right caudal lobes (Fig. 3A, Fig. S1G, Movies 2,3). Conversely, increasing smooth muscle wrapping reduced the frequency of

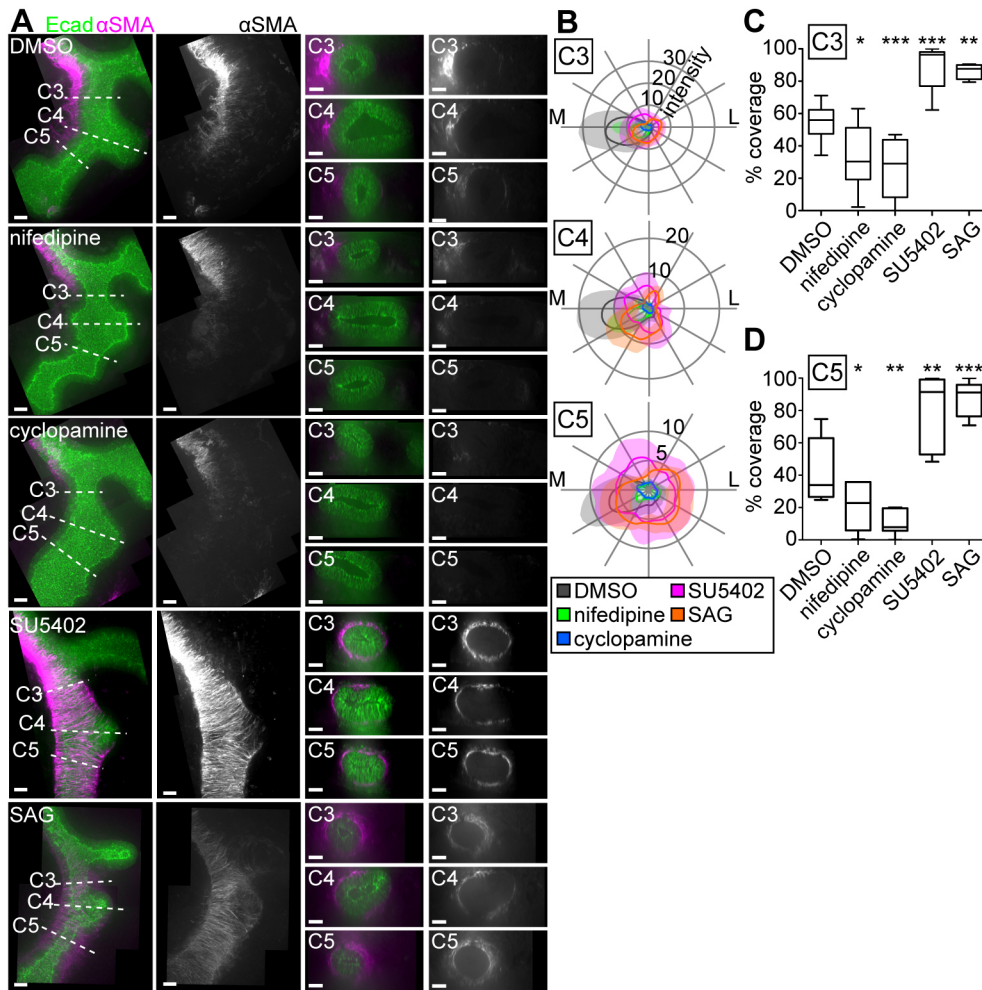


Fig. 2. Pharmacological perturbation of smooth muscle differentiation disrupts smooth muscle coverage.

(A) z-projections and reconstructed cross-sections of the left lobe of lungs isolated at E11.5 and then immunostained for Ecad and α SMA after treatment with DMSO, nifedipine (10 μ M), cyclopamine (1 μ M), SU5402 (10 μ M) or SAG (0.5 μ g/ml) for 24 h. Cross-sections are from locations C3–C5 as indicated in the left-most image. Scale bars: 25 μ m. (B) Polar plots showing mean α SMA intensity relative to background intensity at C3, C4 and C5 for each treatment. Dark lines show mean and shaded regions show s.d. ($n=4-11$). (C,D) Quantification of α SMA coverage around the airway (percentage of airway circumference with above-threshold α SMA signal) at C3 (C) and at C5 (D) for each treatment ($n=4-11$). Boxes show 25th to 75th percentiles; whiskers show minimum and maximum values. *** $P<0.0001$, ** $P<0.001$, * $P<0.05$.

branch initiation (Fig. 3A, Fig. S1G, Movies 4,5) and dramatically slowed the rate of extension of the few branches that did form (Fig. 3B,C, Fig. S1H, Movies 2-5). When smooth muscle wrapping around the epithelium was decreased, narrowing of the domain branch was impaired (Fig. 3B,D, Fig. S1I, Movies 2,3). When smooth muscle wrapping around the epithelium was increased, branch thinning proceeded at a normal rate (Fig. 3B,D, Fig. S1I). Altering smooth muscle coverage around the primary bronchus affects the morphology of the branch; these data suggest that the pattern of smooth muscle differentiation physically shapes emerging domain branches.

To visualize smooth muscle differentiation during domain branch formation, we conducted live imaging of lungs explanted from α SMA-RFP reporter mice. To quantify α SMA-RFP intensity, we traced a thick line along the lateral side of the left lobe at each time point and measured mean signal intensity within the thick line (shaded area in Fig. 3E). We found that in control explants, α SMA-RFP intensity steadily increased proximal and distal to the emerging branch (Fig. 3E,F). In lungs treated with nifedipine or cyclopamine, α SMA-RFP intensity increased in regions proximal but not distal to the branch (Fig. 3G–J). Conversely, in lungs treated with SU5402 or SAG, α SMA-RFP increased dramatically along the length of the lobe but without the clear proximal-distal pattern observed in control lungs (Fig. 3K–N). These data demonstrate that the patterns of smooth muscle observed in fixed lungs (Fig. 2A) arise over the course of domain branching and that smooth muscle differentiation accompanies changes in epithelial morphology.

Mesenchyme-specific disruptions to smooth muscle differentiation

To control for the possibility that our pharmacological treatments had pleiotropic effects on the airway epithelium, we used an adenoviral approach to target mesenchymal cells specifically. We previously found that the airway epithelium is refractory to recombinant adenovirus, which only transduces the mesenchyme (Hsu et al., 2012; Kim et al., 2015). Transducing with a recombinant adenovirus that encodes for shRNA against serum response factor (SRF) (referred to here as shSRF) prevented smooth muscle differentiation in mouse embryonic lung explants (Fig. S5A–D). shSRF-transduced lungs exhibited no net change but more variance in the positioning of branches L.L1 and L.L2 (Fig. S5E–H). Depletion of SRF also affected branch morphology: branches were the same length but were wider at their bases than controls (Fig. S5I,J). This morphology is consistent with that of the branches that form when smooth muscle differentiation is inhibited pharmacologically.

Genetic ablation of nascent smooth muscle cells alters domain branching

Manipulating smooth muscle differentiation *in vivo* can have severe effects on the embryo; for example, Shh-null embryos form lung rudiments that fail to form branches (Pepicelli et al., 1998). Therefore, to disrupt smooth muscle differentiation genetically, we used tissue-specific Cre recombinase to express the human diphtheria toxin receptor (Rosa26-iDTR) in smooth muscle cells and treated lungs *ex vivo* with diphtheria toxin (DT) to ablate airway

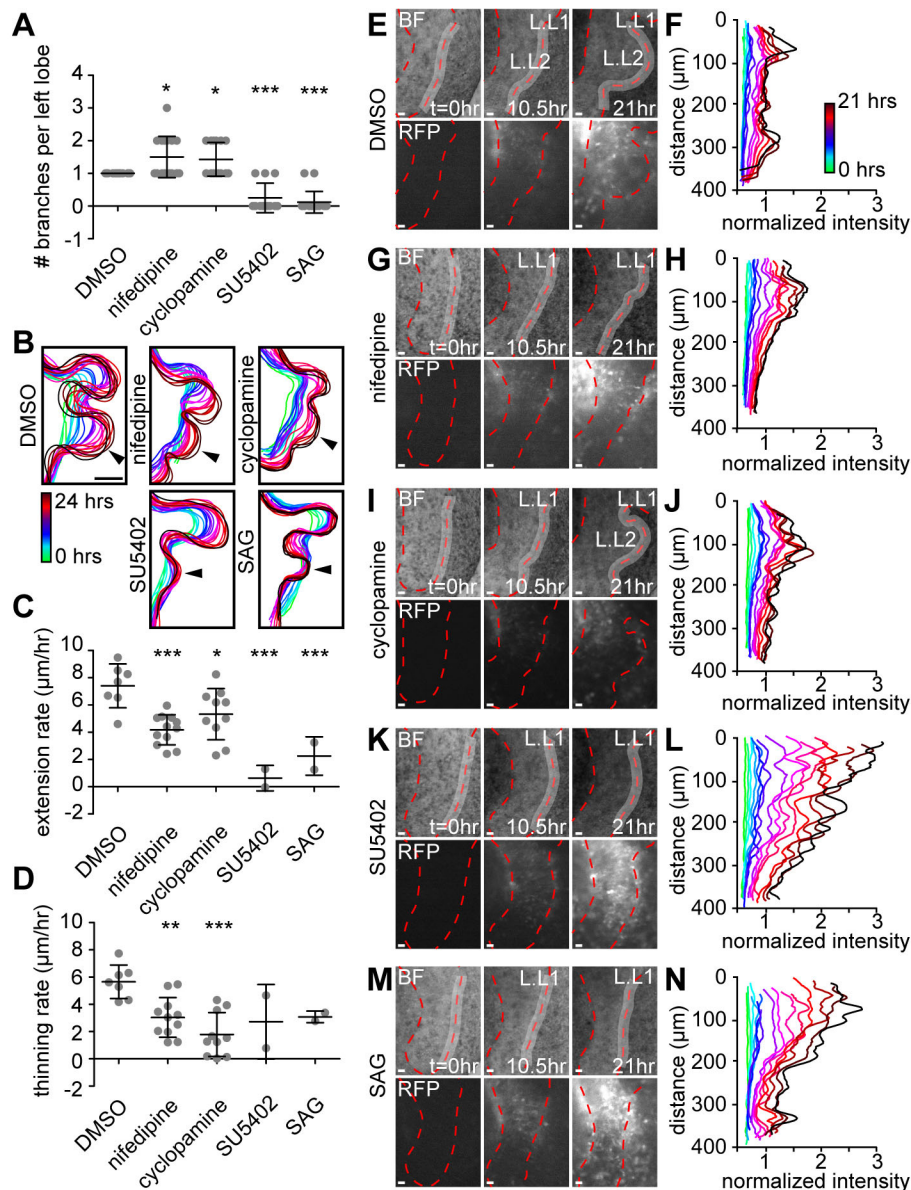


Fig. 3. Smooth muscle differentiation controls the frequency of domain branching and morphology of emerging branches. (A) Number of branching or buckling events occurring over 24 h time-lapse imaging in the left lobe after treatment with either DMSO, nifedipine (10 μM), cyclopamine (1 μM), SU5402 (10 μM) or SAG (0.5 $\mu\text{g/ml}$) ($n=11-17$). (B) Contours of left lobe over the course of a 24 h time-lapse for each treatment. Contours are 1 h apart. Arrowheads indicate branch L.L2. (C,D) Rate of change of length (C) and width (D) of domain branch L.L2 during 24 h time-lapse imaging of treated lungs ($n=2-12$). Only 2/12 SU5402 and 2/17 SAG-treated lungs formed branches over the course of 24 h time-lapses, so only two are plotted. (E-M) Time-lapse imaging and quantification of RFP intensity of $\alpha\text{SMA-RFP}$ lungs treated with DMSO (E,F), nifedipine (G,H), cyclopamine (I,J), SU5402 (K,L) or SAG (M,N). Error bars indicate s.d.; BF indicates brightfield image. *** $P < 0.0001$, ** $P < 0.001$, * $P < 0.05$. Scale bars: 25 μm .

smooth muscle selectively (Fig. 4A, Fig. S7A). We used Acta2-Cre (also known as $\alpha\text{SMA-Cre}$) or Myh11-Cre,-EGFP to achieve specific expression of iDTR in nascent or mature smooth muscle, respectively. Lung explants were isolated at E11.5 and treated with DT for 24 h. We found that after treatment with DT, lungs from Acta2-Cre/+; Rosa26-iDTR fl/+ embryos had reduced smooth muscle coverage distal but not proximal to L.L2, compared with lungs from littermate Rosa26-iDTR fl/+ embryos (Fig. 4B-E) and PBS-treated controls (Fig. S6A,B). Genetic ablation of nascent smooth muscle impeded bifurcations in branch L.L1 and in the right cranial lobe, resulting in a greater fraction of buds in the rounded stages than in the flattened or bifurcated stages compared with controls (Fig. S6B,C). Branch position and the number of new branches in the left lobe after 24 h of culture were unaffected by either genotype or DT treatment (Fig. S6B,D-F), but branch morphology was disrupted in DT-treated Acta2-Cre/+; Rosa26-iDTR fl/+ lungs, as evidenced by reduced length and increased width compared with controls (Fig. 4F,G). These data indicate that genetic ablation of nascent smooth muscle cells mimics the effects

of pharmacological blockade of smooth muscle differentiation in the embryonic mouse lung.

To deplete mature smooth muscle cells, we carried out similar experiments with lungs isolated from Myh11-Cre,-EGFP/+; Rosa26-iDTR fl/+ embryos. After treatment with DT, smooth muscle was lost from around the trachea and the primary bronchus proximal to L.L1; however, we found no significant differences in smooth muscle coverage proximal or distal to L.L2 compared with Rosa26-iDTR fl/+ embryos or PBS-treated controls (Fig. S7B-D). Accordingly, there were no differences in branch position, number, length or width between DT-treated Myh11-Cre,-EGFP/+; Rosa26-iDTR fl/+ embryos and controls (Fig. S7B,E-H). These data suggest that ablation of mature smooth muscle cells, which express Myh11 after the adjacent epithelium has already branched, does not affect epithelial morphology. As expected from the pattern of smooth muscle ablation, we found that *Myh11*-driven EGFP expression is only detectable in the most proximal smooth muscle cells (Fig. S2A), consistent with the fact that the *Myh11* promoter is mainly activated in mature smooth muscle. This expression pattern contrasts that of

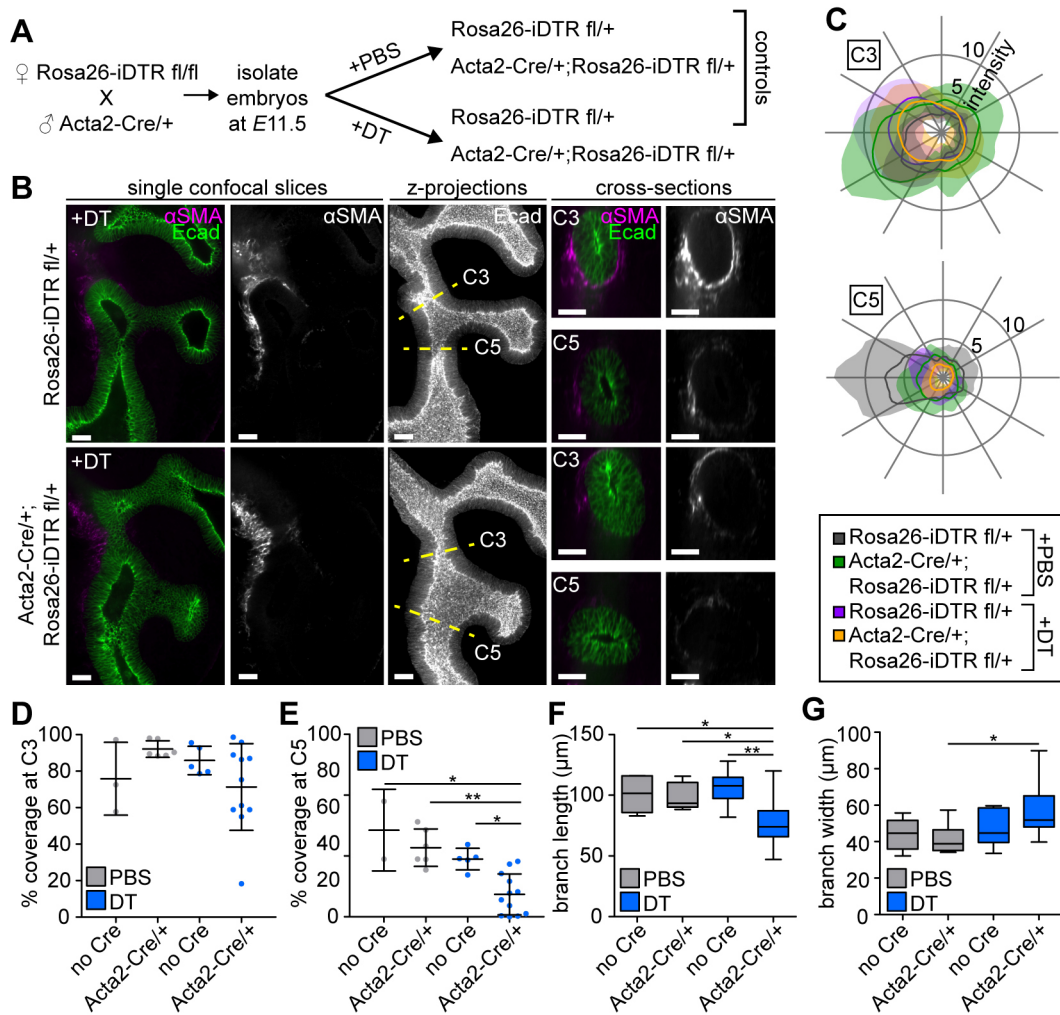


Fig. 4. Genetic ablation of smooth muscle cells impairs domain branching. (A) Experimental scheme: Rosa26-iDTR fl/fl females are mated with Acta2-Cre/+ males. Embryos were isolated at E11.5 for *ex vivo* lung culture. Embryos of both possible genotypes were treated with either PBS or DT for 24 h. (B) Single confocal slices, z-projections, and reconstructed cross-sections of the left lobe of Rosa26-iDTR fl/+ (control) and $\text{Acta2-Cre/+; Rosa26-iDTR fl/+}$ lungs isolated at E11.5 and then immunostained for αSMA and Ecad after treatment for 24 h with 0.2 ng/ μl DT (images of PBS controls are in Fig. S6). Cross-sections are from locations C3 and C5 as indicated in the middle image. Scale bars: 25 μm . (C) Polar plots showing mean αSMA intensity relative to background intensity at C3 and C5 for treated lungs and all controls. Dark lines show mean and shaded regions show s.d. (D,E) Quantification of αSMA coverage around the airway at C3 (D) and C5 (E) ($n=2-12$). (F,G) Length (F) and width (G) of domain branch L.L2 after 24 h culture ($n=5-13$). All genotypes indicated on plots include Rosa26-iDTR fl/+ . * $P<0.05$, ** $P<0.001$.

RFP expressed under the αSMA promoter: RFP-positive cells were detected around the epithelium even in newly committed smooth muscle cells where robust αSMA protein was not yet detectable by immunostaining (Fig. S2B). These data suggest that the coordinated timing of smooth muscle differentiation around the growing epithelium is necessary for sculpting domain branches.

Local epithelial proliferation is complementary to patterns of smooth muscle coverage

Our data thus far demonstrate a clear requirement for smooth muscle differentiation in sculpting emerging domain branches. We next sought to define the possible mechanisms by which smooth muscle influences epithelial morphology. Smooth muscle differentiation could guide branches by altering local epithelial behaviors, such as proliferation, or it could act at the tissue level by either passively guiding or actively squeezing the epithelium into shape. To investigate these possibilities, we first examined epithelial cell proliferation in the distal left lobe over the course of branch

formation. We conducted 5-ethynyl-2'-deoxyuridine (EdU)-pulse experiments on lungs isolated at E11.5, E12 and E12.5 and compared the pattern of epithelial proliferation with the morphology of L.L2 (Fig. 5A, Fig. S8A). We found that the angular distribution of EdU-positive cells in the vicinity of L.L2 evolves over time (Fig. 5B, Fig. S8B). Proximal and distal to L.L2 (regions C3 and C5), there was more proliferation on the lateral side of the primary bronchus at E11.5, and the distribution became more uniform towards E12.5. Conversely, at the level of L.L2 (region C4), the distribution became increasingly skewed towards the lateral side over time. By comparing the mean number of proliferating cells along the lateral surface of the epithelium (normalized to epithelial area), we observed that at E11.5 proliferation is uniform along the lobe, but that by E12.5 proliferation is reduced in the primary bronchus adjacent to L.L2 (Fig. 5C). As the branch grew (and the ratio of length to width increased), epithelial proliferation decreased proximal and distal to L.L2, but remained constant within L.L2 (Fig. 5D-F). These data suggest that the lateral epithelium of the

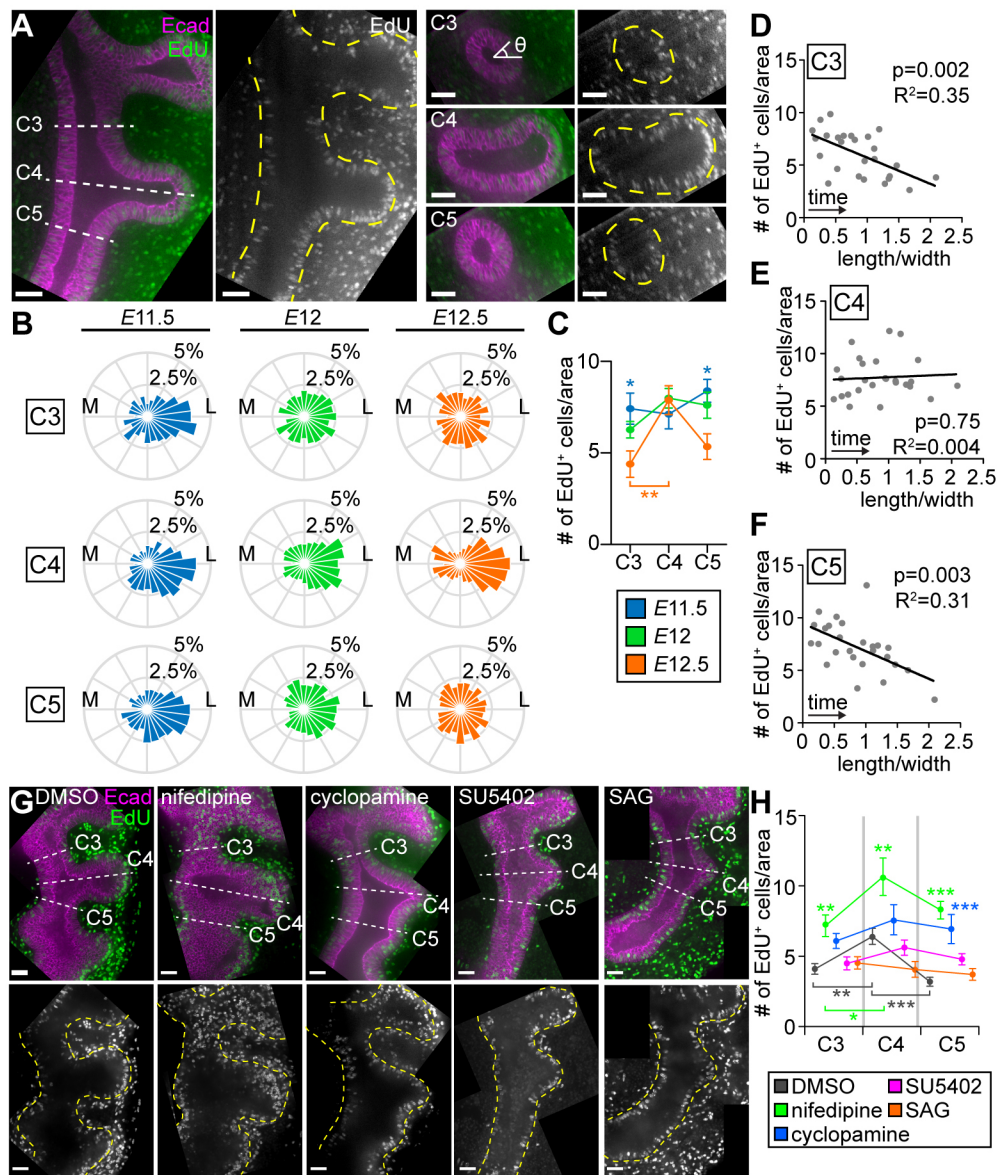


Fig. 5. Patterns of epithelial proliferation in the left lobe evolve during branch formation. (A) z-projections and reconstructed cross-sections of the left lobe of E12 lungs after 30 min EdU pulse and immunostaining for Ecad. Cross-sections are from locations C3-C5 as indicated in the left-most image. Angular position with respect to the center of the primary bronchus is indicated as θ . (B) Angular distribution of EdU⁺ cells with respect to the center of the primary bronchus at cross-sections C3-C5 measured from lungs at E11.5, E12 and E12.5 ($n=7-12$). The radial axis represents the percentage of all cells within each angular bin. (C) Mean number of EdU⁺ cells in the lateral epithelium per 1000 μm^2 of epithelial area at each location C3-C5 and at each developmental stage ($n=7-12$). The lateral epithelium is defined as the region within 45° above or below the medial-lateral axis and with respect to the center of the parent branch. Error bars indicate s.e.m. Asterisks shown above data points reflect comparisons between stages in a given region; asterisks shown below data points reflect comparisons between regions for a given developmental stage. (D-F) Number of EdU⁺ cells in the lateral epithelium per 1000 μm^2 of epithelial area at each location C3-C5 along the branch, plotted against the ratio of length to width of branch L.L2. Results of linear regression including P -value and R^2 values are indicated on each plot ($n=26$). (G) z-projections of the left lobe after a 30 min EdU pulse and immunostaining for Ecad, following treatment with DMSO, nifedipine (10 μM), cyclopamine (1 μM), SU5402 (10 μM) or SAG (0.5 $\mu\text{g}/\text{ml}$) for 24 h. (H) Number of EdU⁺ cells in the lateral epithelium per 1000 μm^2 of epithelial area at each location (C3-C5) and for each treatment ($n=6-14$). Error bars indicate s.e.m. Asterisks shown above data points reflect comparisons between treatment conditions and the DMSO control in a given region; asterisks shown below data points reflect comparisons between regions within each treatment group. Scale bars: 25 μm . Dashed lines in A and G outline the airway epithelium. *** $P<0.0001$, ** $P<0.001$, * $P<0.05$.

distal left lobe is initially uniformly proliferative, but that as the domain branch extends (and as smooth muscle differentiates around the primary bronchus), proliferation becomes restricted to the elongating branch. Further, spatial and temporal patterns of epithelial proliferation are complementary to patterns of smooth muscle coverage around the primary bronchus.

We next examined epithelial proliferation in lungs isolated at E11.5 and treated for 24 h with drugs that alter smooth muscle

differentiation. We found that perturbing smooth muscle differentiation disrupts the spatiotemporal pattern of EdU-positive epithelial cells (Fig. S9). Proliferation rates in the lateral epithelium were increased in the vicinity of L.L2 in nifedipine-treated lungs, particularly distal to L.L2 (Fig. 5G,H). Cyclopamine-treated lungs also showed increased lateral epithelial proliferation distal to L.L2 (Fig. 5G,H). Lungs treated with SU5402 or SAG showed no significant change in proliferation (Fig. 5G,H). These results

suggest that in the absence of patterned smooth muscle, proliferation in the distal left lobe may remain elevated during branch extension. Further, control lungs are the only group in which proliferation is significantly enriched within L.L2 (region C4) compared with the adjacent tissue (region C5) (Fig. 5H). Overall, it appears that disrupting smooth muscle coverage affects patterns of epithelial proliferation in the distal left lobe during domain branching. However, given that these patterns of proliferation arise after branches initiate and that the pharmacological inhibitors have limited effects on the overall rate of proliferation in the epithelium, it remains unclear whether the changes in proliferation affect domain branch initiation.

Morphology, but not volume, of the left lobe is controlled by smooth muscle differentiation

Our alternative (but not mutually exclusive) hypothesis was that smooth muscle could physically squeeze the epithelium into shape. If this were the case, we might expect to observe changes in the morphology of the primary bronchus coincident with domain branch initiation. We therefore measured the width of the primary bronchus over the course of morphogenesis as a readout of smooth muscle-driven constriction. We found that the width of the primary bronchus proximal to L.L2 (region C3) decreased as the branch formed, whereas the width of the bronchus distal to L.L2 (region C5) did not change (Fig. 6A-C), consistent with the proximal-to-distal pattern of smooth muscle differentiation. When smooth muscle differentiation was blocked with cyclopamine, the width of the bronchus proximal to L.L2 decreased at a slower rate (Fig. 6B). In both nifedipine- and cyclopamine-treated lungs, the bronchus distal to L.L2 expanded (Fig. 6C). Conversely, when smooth muscle differentiation was enhanced, the bronchus showed normal thinning at locations proximal to L.L2 and increased thinning distal to L.L2 compared with controls (Fig. 6B,C). Overall, the extent of smooth muscle coverage correlates with changes in the diameter of the primary

bronchus, suggesting a role for smooth muscle mechanics in physically shaping the left lobe of the lung. Indeed, we found that surgically removing the mesenchyme and smooth muscle from the epithelium near L.L2 caused the primary bronchus to spontaneously expand in width (Fig. 6D-G). In lungs that had already formed L.L2, the narrower shape of the bronchus was lost immediately when the mesenchyme was surgically removed (Fig. 6E). These results suggest that in the absence of the surrounding mesenchyme and smooth muscle, the epithelium relaxes and branched morphology is lost.

If smooth muscle contractility defines epithelial morphology, then the volume of the lower left lobe should be conserved across treatments. To test this, we measured the volume of the left lobe distal to L.L1 after 24 h of culture (Fig. 6A,H) and found that volume is conserved between DMSO-treated controls and both nifedipine- and cyclopamine-treated lungs (Fig. 6H). These data suggest that overall epithelial growth is similar under each condition, but that the pattern of smooth muscle differentiation shapes the growing epithelium into domain branches. When smooth muscle differentiation was enhanced, we found that the volume of the distal left lobe was reduced (Fig. 6H); in these lungs, the entire proximal-distal axis of the lobe became surrounded by ectopic smooth muscle, which may inhibit not just domain branching but also elongation of the distal tip of the primary bronchus, resulting in reduced epithelial growth.

Computational modeling reveals that smooth muscle constrains epithelial growth during domain branching

Thus far, our experimental data reveal that epithelial proliferation is enhanced on the lateral side of the epithelium and that disrupting the pattern of smooth muscle differentiation leads to aberrant branching. In order to disentangle the relative roles of patterned growth and smooth muscle differentiation in the proper formation of new domain branches, we constructed a computational model based

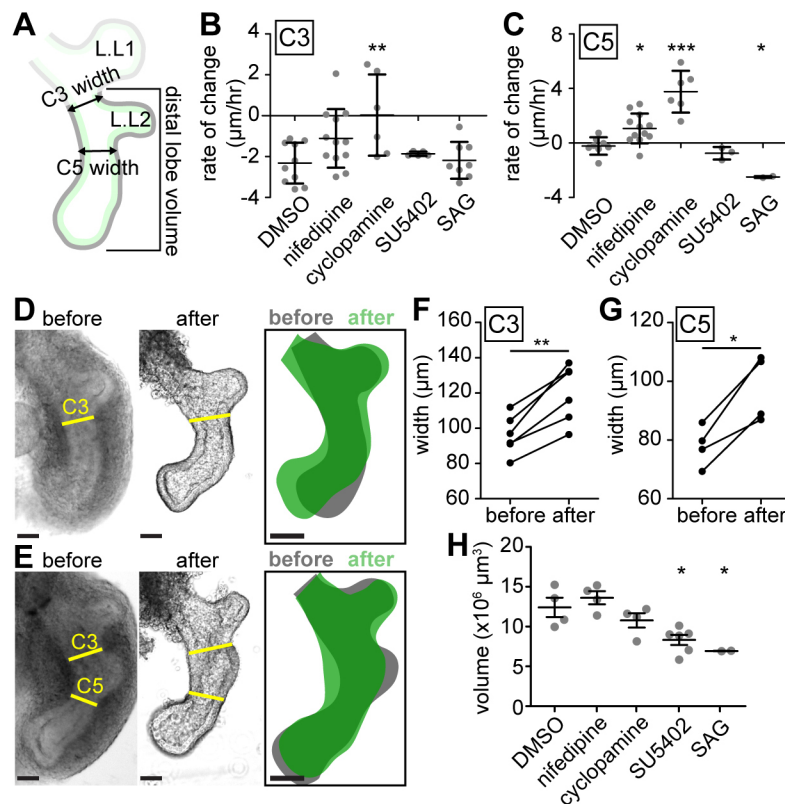


Fig. 6. Effects of smooth muscle on bronchus morphology during domain branching. (A) Schematic of the left lobe showing where bronchial width and volume of the distal lobe are measured in subsequent plots. (B,C) Rate of change of bronchial width at C3 (B) and C5 (C) measured over 24 h time-lapse imaging of lungs treated with DMSO, nifedipine (10 μM), cyclopamine (1 μM), SU5402 (10 μM) or SAG (0.5 μg/ml) ($n=3-12$). (D,E) Images and schematics showing the morphology of the left lobe before and immediately after the mesenchyme has been surgically removed from the epithelium for two samples at early and late stages of L.L2 formation. C3 and C5 cross-sections are indicated. Scale bars: 25 μm. (F,G) Width of the primary bronchus at C3 (F) and C5 (G) before and after removal of the mesenchyme of E11.5 and E12 lungs ($n=4-6$). Connected points represent single samples. (H) Volume of the left lobe measured from the end of L.L1 to the distal tip in each treatment ($n=2-6$). Error bars represent s.d. *** $P<0.0001$, ** $P<0.001$, * $P<0.05$.

on continuum mechanics of growing tissues (Supplementary Materials and Methods; Fig. 7A). For simplicity, we assumed that all tissues (epithelium, mesenchyme and smooth muscle) are completely elastic, because we focused only on the initial stages of domain branch formation when viscoelastic effects of the tissues can be neglected. We modeled differentiation of the mesenchyme into airway smooth muscle as a gradual increase in tissue stiffness (Fig. 7B), because differentiation and contraction both lead to stiffening of the tissue, which is sufficient to represent the smooth muscle layer in other systems (Hrousis et al., 2002; Koyama et al., 2016; Li et al., 2011; Shyer et al., 2013). The initial and the final patterns of smooth muscle wrapping were chosen to mimic our experimental observations (Figs 1E-G and 7B). We assumed that both epithelial growth and smooth muscle differentiation are much slower than mechanical relaxation, and therefore that the growing system is in a quasi-mechanical equilibrium at all times.

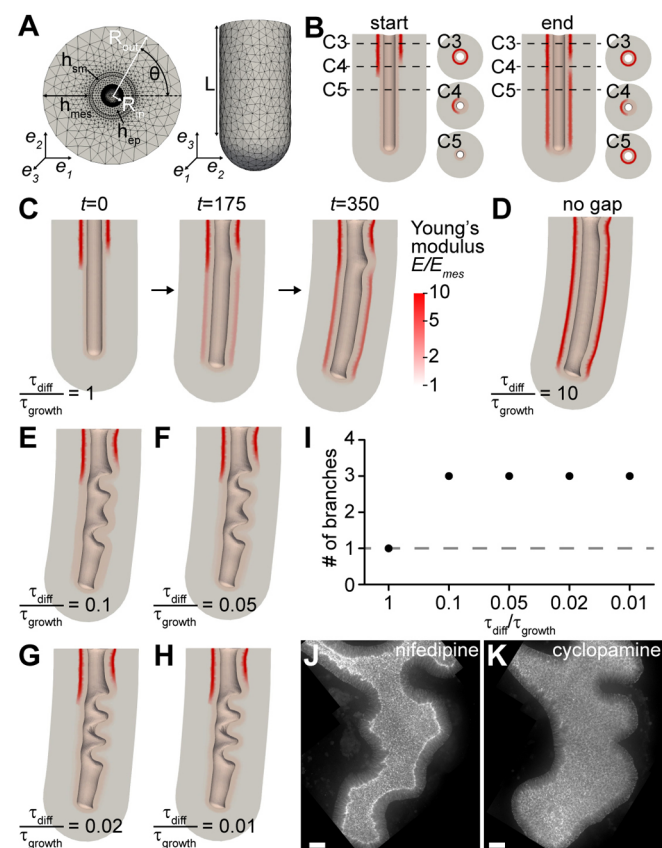


Fig. 7. A computational model of domain branching demonstrates that smooth muscle constrains the growing epithelium into domain branches. (A) Geometry and mesh structure of the model from two different angles. (B) Implementation of smooth muscle layer (red) including starting and ending configurations, and relevant cross-sections corresponding to those introduced in Fig. 1. (C) Snapshots at different times (t) in a simulation in which a single domain branch forms through a gap in the stiff smooth muscle layer. Growth of the epithelium is three times faster on the lateral (right) than on the medial (left) side and the rates of smooth muscle differentiation and epithelial growth are equal ($\tau_{diff}/\tau_{growth}=1$). (D) Snapshot of the final state of a simulation with no gap in the smooth muscle layer and with enhanced smooth muscle differentiation ($\tau_{diff}/\tau_{growth}=10$). (E-H) Final state of simulations in which smooth muscle differentiation is impaired, with $\tau_{diff}/\tau_{growth}=0.1$ (E), 0.05 (F), 0.02 (G) and 0.01 (H). (I) Quantification of the number of lateral branches in simulations with different values of τ . (J, K) Examples of nifedipine (J)- and cyclopamine (K)-treated lungs immunostained for Ecad in which multiple buckles and/or branches formed after 24 h. Scale bars: $25 \mu\text{m}$.

We began by assuming that the epithelium grows faster on the lateral side of the primary bronchus than on the medial side, based on our experimental observations of DNA synthesis in lung explants (Fig. 5B). Our model revealed that the epithelium forms into domain branches when the differentiation rate of smooth muscle is roughly the same order of magnitude as the growth rate of the epithelium (Fig. 7C; Movie 6). The number of domain branches formed by the epithelium depends on the pattern of smooth muscle differentiation, with larger gaps in smooth muscle coverage yielding proportionally more branches (Fig. S10A,B). When smooth muscle differentiation is much faster than the rate of epithelial growth, branches are unable to form (Fig. 7D). However, when the rate of smooth muscle differentiation is impaired in the model, stresses that build up in the growing epithelial tissue are released as a wrinkling instability: periodic patterns of domain branches form simultaneously on the lateral side of the primary bronchus and, subsequently, additional branches can form on the medial side (Fig. 7E-I; Fig. S10C; Movies 7-8). This is akin to the wrinkling instability observed during the development of the brain (Budday et al., 2015a,b; Tallinen et al., 2014, 2016) and the gut (Shyer et al., 2013). Importantly, the simulated epithelium produces ectopic branches or wrinkles instead of single-domain branches as the rate of smooth muscle differentiation approaches zero (Fig. 7H; Movie 8). These ectopic branches are reminiscent of those that form experimentally when lungs are treated with nifedipine or cyclopamine (Fig. 7J,K).

Experimentally disrupting proliferation within the embryonic lung blocks the formation of domain branches (Goldin et al., 1984), but it is unclear whether local patterns of epithelial growth are necessary for branching morphogenesis. To test the role of patterned proliferation in domain branching, we next abolished the lateral bias in epithelial growth and instead modeled the epithelium as a uniformly growing tissue. Under these conditions, we again found that domain branches form properly on the lateral side of the bronchus when the relative rate of epithelial growth matches the rate of smooth muscle differentiation (Fig. S10D). When the rate of smooth muscle differentiation is reduced, the epithelium buckles into the surrounding mesenchyme and forms ectopic branches on both sides of the bronchus. The results of these simulations suggest that the pattern of airway smooth muscle differentiation mechanically guides the growing epithelium into domain branches (Fig. 8), and that epithelial growth alone is insufficient for the proper initiation and shaping of branches.

DISCUSSION

Our study reveals an essential role for airway smooth muscle in sculpting emerging domain branches in the embryonic mouse lung. We have shown that domain branching is highly stereotyped and accompanied by evolving spatial patterns of smooth muscle. Perturbing these patterns of differentiation with pharmacological, adenoviral or genetic approaches disrupts domain branching. Enhanced wrapping of smooth muscle around the epithelium suppresses branch initiation and extension, whereas decreased smooth muscle coverage reduces positional stereotypy and leads to the formation of ectopic branches as a result of epithelial buckling (Varner et al., 2015). Ablation of smooth muscle cells at early stages of differentiation affects domain branching. Based on these findings, we propose that domain branches are sculpted as smooth muscle differentiates. We found that pharmacological perturbations to smooth muscle differentiation do not drastically affect epithelial proliferation, but regional differences in epithelial proliferation are likely an indirect result of abnormal branching when smooth muscle differentiation is perturbed. Instead, we found that the overall morphology of the left lobe is regulated by smooth muscle

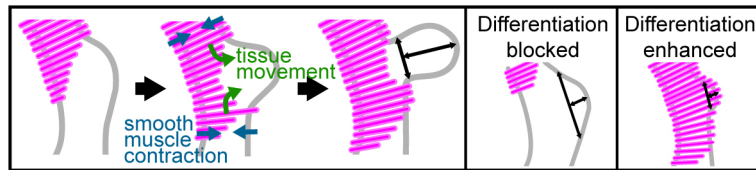


Fig. 8. Proposed model: differentiation of smooth muscle around the primary bronchus leads to thinning of elongating branches by physical constriction of the epithelium. As the airway epithelium expands, patterned smooth muscle differentiation and contraction guide/squeeze it into the correct branched morphology. When smooth muscle differentiation is blocked, the epithelium grows outward but its growth is unconstrained and the distal left lobe becomes dilated and then buckles. When smooth muscle differentiation is enhanced, a sheath of smooth muscle envelops the entire distal left lobe, preventing branch initiation and extension.

differentiation during branch formation. Specifically, the primary bronchus adjacent to an emerging branch is gradually constricted, and this thinning depends on smooth muscle differentiation. Finally, we found that the volume of the airway is conserved even when smooth muscle differentiation is disrupted. Combined with our simulations, these data suggest a model in which the airway epithelium expands uniformly into the mesenchyme and is guided into a branched morphology by spatially patterned smooth muscle differentiation (Fig. 8). The local presence of newly differentiated smooth muscle appears to exert a physical force to direct the expansion of the growing epithelium.

These findings contrast with the mechanisms by which domain branches form in the avian lung. In the embryonic chicken, apical constriction (but not proliferation) of the epithelium is required for domain branch initiation (Kim et al., 2013; Tzou et al., 2016). These earliest stages of avian lung development occur in the absence of airway smooth muscle (Spurlin et al., 2019); it thus appears that avian and murine lungs employ divergent mechanisms to form domain branches. Although trapezoid-shaped cells have been detected in the embryonic mouse lung, it is unclear whether active apical constriction takes place during domain branching. Inhibiting RhoA results in reduced branching and dilated epithelial tips (Kadzic et al., 2014); although this inhibition might prevent changes in epithelial cell shape, it would also be expected to disrupt smooth muscle differentiation (Mack et al., 2001; Zhao et al., 2007) and contractility (Ihara et al., 2015; Martinsen et al., 2014).

Smooth muscle directs epithelial morphogenesis in other organs, including the chicken intestine (Shyer et al., 2013). Differentiation of circumferential and longitudinal smooth muscle around the gut generates compressive forces that cause buckling of the intestinal epithelium (Shyer et al., 2013). Buckling has also been observed in mesenchyme-free lung explants (Varner et al., 2015); compressive forces generated by a proliferating epithelium surrounded by mesenchyme and airway smooth muscle might lead to bending of the epithelium and subsequent branch formation. Branching morphogenesis of the mouse prostate also involves smooth muscle differentiation; mouse models with activated Shh signaling have increased smooth muscle around epithelial ducts and reduced lateral branching (Leow et al., 2009). This defect is similar to what we observed here in lung explants treated with SAG. Smooth muscle-like tissues, including myofibroblasts and myoepithelium, have also been shown to direct epithelial morphogenesis during alveologenesis in the lung (Branchfield et al., 2016) and during branch elongation in mammary organoids (Neumann et al., 2018). The instructive role played by smooth muscle and smooth muscle-like tissues surrounding developing epithelia might be a common developmental motif used during organogenesis.

After lateral domain branches have formed, the left and right caudal lobes of the murine lung develop domain branches on their dorsal, medial and ventral sides (Metzger et al., 2008). These

nascent domain branches recruit new smooth muscle progenitors from the surrounding mesenchyme that are of a different lineage than the smooth muscle that already surrounds the parent branch (Kumar et al., 2014). Initiation of these branches must involve elimination or remodeling of the existing smooth muscle sheath. It is likely, therefore, that smooth muscle differentiation regulates formation of these branches as well; indeed, pharmacological enhancement of smooth muscle differentiation appears to block initiation of dorsal domain branches in the left lobe, whereas blocking smooth muscle differentiation leads to ectopic branches that extend dorsally or medially (Fig. S4A; Kim et al., 2015).

How does the lung achieve the specific spatial patterns of smooth muscle required for normal epithelial branching? Shh secreted by the epithelium and Fgf9 secreted by the mesothelium could establish gradients of induction and suppression of smooth muscle differentiation across the thickness of the pulmonary mesenchyme. However, this broad gradient is unlikely to explain the finer patterns of smooth muscle differentiation described here. Morphogen gradients can be modified by local tissue geometry (Manning et al., 2015; Shyer et al., 2015), and it is possible that epithelial growth or bending could shape the local concentrations of Shh or Fgf9 to favor specific patterns of smooth muscle differentiation. Complex morphogen landscapes can also be established through the combined activities of multiple signaling pathways, as has recently been demonstrated in the murine gut mesenchyme wherein hedgehog-induced smooth muscle differentiation can be halted by nuclear YAP (Cotton et al., 2017). YAP is detectable in the nuclei of pulmonary mesenchymal cells (Cotton et al., 2017), but studies of YAP signaling in lung development have focused primarily on the airway epithelium (Lange et al., 2015; Lin et al., 2017). It will be interesting to determine whether YAP or other known mechanotransducers play a role in spatial patterning of smooth muscle differentiation in the mouse lung. Finally, epithelial outgrowth could generate strain in the mesenchyme that leads to mechanical stress patterns that induce airway smooth muscle differentiation. Stretching undifferentiated mesenchymal cells in culture can induce the expression of smooth muscle proteins and myogenesis (Yang et al., 2000), and increasing transmural pressure in embryonic lung explants (thus increasing pushing forces from the epithelium into the mesenchyme) enhances differentiation of airway smooth muscle (Nelson et al., 2017). Spatially controlled smooth muscle differentiation is likely regulated by a combination of molecular and mechanical factors.

Genetic studies have shown that disrupting Shh signaling leads to hypoplastic lungs with dilated epithelial tips and reduced branching (Boucherat et al., 2015; He et al., 2017; HERRIGES et al., 2015). There are multiple physical mechanisms that could produce these phenotypes, including forces intrinsic to the epithelium, basement membrane compliance, or smooth muscle coverage. Given that Shh signaling is required for smooth muscle differentiation, it is possible that loss of smooth muscle coverage causes hypoplastic phenotypes.

For example, deleting the heparin sulfate synthetase *Ext1* in the epithelium decreases the amount of biologically active Shh protein and results in reduced branching and dilated epithelial tips (He et al., 2017). These mutant lungs also show a reduction in smooth muscle coverage, and treatment with SAG rescues tip dilation, possibly by restoring smooth muscle differentiation, although this was not specifically tested by the authors. To define a role for smooth muscle in hypoplastic Shh phenotypes, future studies could attempt to rescue smooth muscle differentiation either by stimulating Shh signaling directly or through an orthogonal pathway, such as FGF9 or SRF, in mutant lungs in which the Shh pathway has been disrupted.

The mechanisms that drive bifurcations and domain branching are debated. FGF10 produced in the mesenchyme and its receptor FGFR2 in the epithelium are absolutely required for branching morphogenesis (Abler et al., 2009; Arman et al., 1999; Min et al., 1998). Some studies have suggested that spatially restricted sources of FGF10 in the mesenchyme act as chemoattractants that direct epithelial outgrowth (Bellusci et al., 1997; Hirashima et al., 2009; Menshykau et al., 2012). This model is widely accepted (Herriges et al., 2015; McCulley et al., 2015; Morrisey and Hogan, 2010; Swarr and Morrisey, 2015), despite key experiments showing that overexpressing FGF10 in FGF10-null embryos, and effectively abolishing any patterns of FGF10 in the mesenchyme, restores normal epithelial branching (Volckaert et al., 2013). Regardless, it is highly unlikely that FGF10 alone serves as the master regulator of epithelial geometry, branch formation, and outgrowth. Patterned proliferation only arises after branches have formed and therefore cannot initiate morphogenesis (Nogawa et al., 1998). Actin filament accumulation, indicative of cellular force generation (such as apical constriction), is not observed in mesenchyme-free epithelial culture until after branches have already formed (Miura and Shiota, 2000). Our data and previous work suggest that rapid growth of the epithelium is constrained by spatially patterned smooth muscle, leading to bifurcation and branch formation. Without this mechanical constraint, the airway epithelium balloons or buckles; these two outcomes are likely dictated by epithelial proliferation rate, as suggested by mesenchyme-free experiments (Varner et al., 2015). Importantly, we find that lungs treated with pharmacological inhibitors that perturb smooth muscle differentiation do not show severe defects in the amount of epithelial proliferation, lending further support to a role for smooth muscle in regulating branching.

Much remains to be uncovered if we are to truly understand the complex relationships between epithelial branching and smooth muscle differentiation and, in particular, how signaling networks and mechanical forces may cooperate to achieve patterned differentiation. Our work reveals a clear spatiotemporal correlation between emerging domain branches and localized smooth muscle differentiation, and points to possible mechanisms by which this pattern of smooth muscle might guide the epithelium into its final morphology. We establish smooth muscle as a crucial regulator of early lung branching morphogenesis, and anticipate that it may play similar roles in other smooth muscle-encircled epithelial tissues.

MATERIALS AND METHODS

Mouse lines

Breeding of CD1, FVB, α SMA-RFP, Myh11-Cre,-EGFP (JAX 007742), Acta2-Cre (JAX 029925) and Rosa26-iDTR (JAX 007900) mice and isolation of embryos was carried out in accordance with institutional guidelines following the NIH Guide for the Care and Use of Laboratory Animals and approved by Princeton's and the Mayo Clinic's Institutional Animal Care and Use Committees. Time-lapse imaging of the α SMA-RFP reporter was carried out in embryos from FVB females bred to heterozygous α SMA-RFP males. Smooth muscle ablation experiments were carried out in

embryos from Rosa26-iDTR homozygous females bred to either Acta2-Cre or Myh11-Cre,-EGFP hemizygous males. Embryos from Myh11-Cre,-EGFP studs were genotyped based on EGFP fluorescence in the lungs. Embryos from Acta2-Cre studs were genotyped by isolating DNA from the head of each embryo, followed by PCR amplification of the Cre product and gel electrophoresis. The forward primer sequence was GCATTACCGGT-CGATGCAACGAGTGATGAG and the reverse primer sequence was GAGTGAACGAACCTGGTCGAAATCAGTGCG.

Organ culture and live imaging

Ex vivo culture of E11.5 lung explants was performed following previously described protocols (Carraro et al., 2010). Lungs were dissected in PBS and cultured on porous membranes (nucleopore polycarbonate track-etch membrane, 8 μ m pore size, 25 mm diameter; Whatman) in DMEM/F12 medium (without HEPES) supplemented with 5% fetal bovine serum (FBS, heat inactivated; Atlanta Biologicals) and antibiotics (50 units/ml of penicillin and streptomycin). Reagents used to perturb smooth muscle differentiation were nifedipine (10 μ M; Sigma-Aldrich), cyclopamine (1 μ M; Tocris), SU5402 (5 μ M; Santa Cruz Biotechnology) and SAG (0.5 μ g/ml; Calbiochem). To disrupt smooth muscle differentiation specifically, explants were transduced with custom recombinant adenoviruses that encoded either a scrambled-sequence control (sh-ctrl) or shRNA against SRF (shSRF) (Vector Biolabs). For genetic ablation of smooth muscle, lungs were isolated from Rosa26-iDTR homozygous females bred to either Acta2-Cre or Myh11-Cre,-EGFP hemizygous males, and then treated with either 0.2 ng/ μ l or 0.5 ng/ μ l DT (Sigma-Aldrich), respectively. Before addition to the culture medium, DT was unnicked by incubating with trypsin at a ratio of 1:10,000 in PBS for 15 min at 37°C. The genotypes and conditions of littermate controls were Rosa26-iDTR fl/+ with PBS, Acta2-Cre/+; Rosa26-iDTR fl/+ with PBS, and Rosa26-iDTR fl/+ with 0.2 ng/ μ l DT. Equivalent controls were used for the Myh11-Cre,-EGFP experiments. For live imaging, lungs were cultured on Transwell filters (polyethylene terephthalate membrane, 3 μ m pore size, 10.5 mm diameter; Corning) within a stage-top incubator (Pathology Devices). Frames were acquired every 30 min (or 90 min for α SMA-RFP) for 24 h under brightfield (1–2 ms exposure per plane for a total of six to eight planes per time point) or epifluorescence (500 ms exposure per plane for a total of four or five planes per time point) on an inverted microscope (Nikon Ti).

Immunofluorescence staining and imaging

Lung explants were fixed with 4% paraformaldehyde in PBS for 15 min at room temperature. Fixation was followed by washing in 0.3% Triton X-100 in PBS and blocking with 5% goat serum and 0.1% bovine serum albumin (BSA). Samples were incubated with primary antibodies against E-cadherin (Cell Signaling 3195, 1:200 or Invitrogen 13-1900, 1:200), α SMA (Sigma-Aldrich a5228, 1:400 or Abcam ab5694, 1:200), GFP (Invitrogen A-11122, 1:500), or RFP (Abcam ab62341, 1:400), followed by incubation with Alexa Fluor-conjugated secondary antibodies (1:200; Thermo Fisher Scientific A11032, A11034, A21240 and A11006). Stained lungs were dehydrated in a methanol series and cleared using Murray's clear (1:2 ratio of benzyl alcohol to benzyl benzoate). Confocal images were collected using a spinning disk confocal (Bio-Rad) fitted to an inverted microscope. EdU assays were conducted using the Click-iT EdU Alexa Fluor 488 Kit (Thermo Fisher Scientific). EdU was added to culture medium for 30 min immediately prior to fixation.

Microdissection to remove mesenchyme

To remove the mesenchyme, embryonic lungs were isolated as described above and then submerged in dispase (Corning) for 5 min at room temperature. Dispase was inactivated by adding medium supplemented with FBS (as described above) and 0.1% BSA. The mesenchyme was then microdissected away from the epithelium using fine tungsten needles (Fine Science Tools). The widths of the primary bronchus before and after dissection were compared using a paired *t*-test in GraphPad Prism 5.

Image analysis and statistics

Quantitative image analysis and image projections were obtained using ImageJ and MATLAB. When necessary, images were stitched together using the Grid/Collection stitching plugin in ImageJ (Preibisch et al., 2009).

To quantify branch positions, lungs were segmented and skeletonized in ImageJ, and then analyzed using the Analyze Skeleton plugin (Arganda-Carreras et al., 2010) to determine distances between the tracheal fork (the proximal end of the left lobe), the branches L.L1 and L.L2, and the distal end of the left lobe, or the distances between the proximal and distal ends of the right caudal lobe and the branch RCd.L1. Relative distance was defined as the position of the branch along the primary bronchus as measured from the tracheal fork (or the proximal end of the lobe) divided by the total length of the lobe. Width and length of branches were manually quantified from time-lapse movies or from images of stained explants. Width was measured at the base of the branch along the primary bronchus, and length was measured from the edge of the primary bronchus to the end of the branch.

Intensity of α SMA around the bronchus was quantified at five positions within each region (C1-C5) by tracing the circumference of the airway epithelium and measuring total signal intensity within a 16×16 pixel ($5.7 \times 5.7 \mu\text{m}$) window at each point along the circumference. For downstream analysis, the mean of all five positions was used. Intensity measurements were normalized to background and binned based on the angle of each point with respect to the center of the bronchus to generate polar plots. Smooth muscle coverage was measured as the percentage of airway circumference with above-threshold α SMA staining intensity. Branching frequency was estimated from time-lapse movies and by counting the number of branching events (defined as a protrusion of the epithelium greater than $15 \mu\text{m}$ away from the edge of the primary bronchus) that occurred in the left lobe over the course of 24 h. For time-lapse analyses, α SMA-RFP intensity was measured along the lateral side of the left lobe by manually tracing from the base of L.L1 to the distal end of the lobe. The mean intensity was measured in a 32×32 pixel ($20.8 \times 20.8 \mu\text{m}$) region around each point of the outline and then normalized to mean intensity of the entire image.

EdU analysis was carried out at five positions within each region of the left lobe (C1-C5) on reconstructed cross-sections through z-stacks. We measured the cross-sectional epithelial area, the number of EdU⁺ cells, and their angular positions with respect to the center of the primary bronchus. Angular distributions of EdU⁺ cells were compared using the Kolmogorov-Smirnov test. To compare local proliferation between developmental groups or drug treatments, we restricted our analysis to the lateral side of the branch (45° above and below the medial-lateral axis through the center of the primary bronchus) and normalized the number of EdU⁺ cells by dividing by epithelial area.

Linear regressions were performed to determine correlations between smooth muscle coverage, the normalized number of EdU⁺ cells, and branch morphology using GraphPad Prism 5. ANOVA was used for comparisons between each treatment in GraphPad Prism 5. Bartlett's test for unequal variances was used to compare variance of relative branch positions in MATLAB.

Computational model

The computational model is described in detail in the supplementary Materials and Methods. To generate the results presented in Fig. 7, we ran simulations in which the rate of epithelial growth was three times faster on the lateral side, and in which the smooth muscle differentiation rate was between 1 and 0.01 times that of the epithelial growth rate.

Competing interests

The authors declare no competing or financial interests.

Author contributions

Conceptualization: K.G., C.M.N.; Methodology: K.G., C.M.N.; Software: S.M., T.G., A.K.; Formal analysis: S.M., T.G., A.K.; Investigation: K.G.; Resources: E.M., D.C.R.; Writing - original draft: K.G., A.K., C.M.N.; Writing - review & editing: K.G., C.M.N.; Supervision: C.M.N.; Project administration: C.M.N.; Funding acquisition: C.M.N.

Funding

This work was funded by the National Institutes of Health (HL120142), the National Science Foundation (CMMI-1435853) and a Faculty Scholars Award from the Howard Hughes Medical Institute. Deposited in PMC for release after 12 months.

Supplementary information

Supplementary information available online at <http://dev.biologists.org/lookup/doi/10.1242/dev.181172.supplemental>

References

- Abler, L. L., Mansour, S. L. and Sun, X. (2009). Conditional gene inactivation reveals roles for Fgf10 and Fgf2 in establishing a normal pattern of epithelial branching in the mouse lung. *Dev. Dyn.* **238**, 1999-2013. doi:10.1002/dvdy.22032
- Arganda-Carreras, I., Fernández-González, R., Muñoz-Barrutia, A. and Ortiz-De-Solorzano, C. (2010). 3D reconstruction of histological sections: application to mammary gland tissue. *Microsc. Res. Tech.* **73**, 1019-1029. doi:10.1002/jemt.20829
- Arman, E., Haffner-Krausz, R., Gorivodsky, M. and Lonai, P. (1999). Fgf2 is required for limb outgrowth and lung-branching morphogenesis. *Proc. Natl. Acad. Sci. USA* **96**, 11895-11899. doi:10.1073/pnas.96.21.11895
- Bellusci, S., Grindley, J., Emoto, H., Itoh, N. and Hogan, B. L. (1997). Fibroblast growth factor 10 (FGF10) and branching morphogenesis in the embryonic mouse lung. *Development* **124**, 4867-4878.
- Boucherat, O., Landry-Truchon, K., Berube-Simard, F.-A., Houde, N., Beuret, L., Lezmi, G., Foulkes, W. D., Delacourt, C., Charron, J. and Jeannotte, L. (2015). Epithelial inactivation of Yy1 abrogates lung branching morphogenesis. *Development* **142**, 2981-2995. doi:10.1242/dev.120469
- Branchfield, K., Li, R., Lungova, V., Verheyden, J. M., McCulley, D. and Sun, X. (2016). A three-dimensional study of alveologenesis in mouse lung. *Dev. Biol.* **409**, 429-441. doi:10.1016/j.ydbio.2015.11.017
- Budday, S., Steinmann, P., Gorieli, A. and Kuhl, E. (2015a). Size and curvature regulate pattern selection in the mammalian brain. *Extreme Mech. Lett.* **4**, 193-198. doi:10.1016/j.eml.2015.07.004
- Budday, S., Steinmann, P. and Kuhl, E. (2015b). Physical biology of human brain development. *Front. Cell Neurosci.* **9**, 257. doi:10.3389/fncel.2015.00257
- Carraro, G., del Moral, P.-M. and Warburton, D. (2010). Mouse embryonic lung culture, a system to evaluate the molecular mechanisms of branching. *J. Vis. Exp.* **40**, 2035. doi:10.3791/2035
- Chen, J. K., Taipale, J., Cooper, M. K. and Beachy, P. A. (2002a). Inhibition of Hedgehog signaling by direct binding of cyclopamine to Smoothened. *Genes Dev.* **16**, 2743-2748. doi:10.1101/gad.1025302
- Chen, J. K., Taipale, J., Young, K. E., Maiti, T. and Beachy, P. A. (2002b). Small molecule modulation of Smoothened activity. *Proc. Natl. Acad. Sci. USA* **99**, 14071-14076. doi:10.1073/pnas.182542899
- Cotton, J. L., Li, Q., Ma, L., Park, J.-S., Wang, J., Ou, J., Zhu, L. J., Ip, Y. T., Johnson, R. L. and Mao, J. (2017). YAP/TAZ and hedgehog coordinate growth and patterning in gastrointestinal mesenchyme. *Dev. Cell* **43**, 35-47.e34. doi:10.1016/j.devcel.2017.08.019
- Ettensohn, C. A. (1985). Mechanisms of epithelial invagination. *Q. Rev. Biol.* **60**, 289-307. doi:10.1086/414426
- Goldin, G. V., Hindman, H. M. and Wessells, N. K. (1984). The role of cell proliferation and cellular shape change in branching morphogenesis of the embryonic mouse lung: analysis using aphidicolin and cytochalasins. *J. Exp. Zool.* **232**, 287-296. doi:10.1002/jez.1402320216
- He, H., Huang, M., Sun, S., Wu, Y. and Lin, X. (2017). Epithelial heparan sulfate regulates Sonic Hedgehog signaling in lung development. *PLoS Genet.* **13**, e1006992. doi:10.1371/journal.pgen.1006992
- Herriges, J. C., Verheyden, J. M., Zhang, Z., Sui, P., Zhang, Y., Anderson, M. J., Swing, D. A., Zhang, Y., Lewandoski, M. and Sun, X. (2015). FGF-regulated ETV transcription factors control FGF-SHH feedback loop in lung branching. *Dev. Cell* **35**, 322-332. doi:10.1016/j.devcel.2015.10.006
- Hirashima, T., Iwasa, Y. and Morishita, Y. (2009). Mechanisms for split localization of Fgf10 expression in early lung development. *Dev. Dyn.* **238**, 2813-2822. doi:10.1002/dvdy.22108
- Hrousis, C. A., Wiggs, B. J. R., Drazen, J. M., Parks, D. M. and Kamm, R. D. (2002). Mucosal folding in biologic vessels. *J. Biomech. Eng.* **124**, 334-341. doi:10.1115/1.1489450
- Hsu, J. C., Di Pasquale, G., Harunaga, J. S., Onodera, T., Hoffman, M. P., Chiorini, J. A. and Yamada, K. M. (2012). Viral gene transfer to developing mouse salivary glands. *J. Dent. Res.* **91**, 197-202. doi:10.1177/0022034511429346
- Ihara, E., Yu, Q., Chappellaz, M. and MacDonald, J. A. (2015). ERK and p38MAPK pathways regulate myosin light chain phosphatase and contribute to Ca²⁺ sensitization of intestinal smooth muscle contraction. *Neurogastroenterol. Motil.* **27**, 135-146. doi:10.1111/nmo.12491
- Jaslove, J. M. and Nelson, C. M. (2018). Smooth muscle: a stiff sculptor of epithelial shapes. *Philos. Trans. R. Soc. Lond. B Biol. Sci.* **373**, 20170318. doi:10.1098/rstb.2017.0318
- Kadzik, R. S., Cohen, E. D., Morley, M. P., Stewart, K. M., Lu, M. M. and Morrisey, E. E. (2014). Wnt ligand/Frizzled 2 receptor signaling regulates tube shape and branch-point formation in the lung through control of epithelial cell shape. *Proc. Natl. Acad. Sci. USA* **111**, 12444-12449. doi:10.1073/pnas.1406639111
- Kim, H. Y., Varner, V. D. and Nelson, C. M. (2013). Apical constriction initiates new bud formation during monopodial branching of the embryonic chicken lung. *Development* **140**, 3146-3155. doi:10.1242/dev.093682
- Kim, H. Y., Pang, M.-F., Varner, V. D., Kojima, L., Miller, E., Radisky, D. C. and Nelson, C. M. (2015). Localized smooth muscle differentiation is essential for epithelial bifurcation during branching morphogenesis of the mammalian lung. *Dev. Cell* **34**, 719-726. doi:10.1016/j.devcel.2015.08.012

- Koyama, H., Shi, D., Suzuki, M., Ueno, N., Uemura, T. and Fujimori, T. (2016). Mechanical regulation of three-dimensional epithelial fold pattern formation in the mouse oviduct. *Biophys. J.* **111**, 650-665. doi:10.1016/j.bpj.2016.06.032
- Kumar, M. E., Bogard, P. E., Espinoza, F. H., Menke, D. B., Kingsley, D. M. and Krasnow, M. A. (2014). Mesenchymal cells. Defining a mesenchymal progenitor niche at single-cell resolution. *Science* **346**, 1258810. doi:10.1126/science.1258810
- Lange, A. W., Sridharan, A., Xu, Y., Stripp, B. R., Perl, A.-K. and Whitsett, J. A. (2015). Hippo/Yap signaling controls epithelial progenitor cell proliferation and differentiation in the embryonic and adult lung. *J. Mol. Cell Biol.* **7**, 35-47. doi:10.1093/jmcb/mju046
- Leow, C. C., Wang, B.-E., Ross, J., Chan, S. M., Zha, J., Carano, R. A. D., Frantz, G., Shen, M. M., de Sauvage, F. J. and Gao, W.-Q. (2009). Prostate-specific Klf6 inactivation impairs anterior prostate branching morphogenesis through increased activation of the Shh pathway. *J. Biol. Chem.* **284**, 21057-21065. doi:10.1074/jbc.M109.001776
- Li, B., Cao, Y.-P. and Feng, X.-Q. (2011). Growth and surface folding of esophageal mucosa: a biomechanical model. *J. Biomech.* **44**, 182-188. doi:10.1016/j.jbiomech.2010.09.007
- Lin, C., Yao, E., Zhang, K., Jiang, X., Croll, S., Thompson-Peer, K. and Chuang, P.-T. (2017). YAP is essential for mechanical force production and epithelial cell proliferation during lung branching morphogenesis. *eLife* **6**, e21130. doi:10.7554/eLife.21130
- Mack, C. P., Somlyo, A. V., Hautmann, M., Somlyo, A. P. and Owens, G. K. (2001). Smooth muscle differentiation marker gene expression is regulated by RhoA-mediated actin polymerization. *J. Biol. Chem.* **276**, 341-347. doi:10.1074/jbc.M005505200
- Manning, L. A., Weideman, A. M., Peercy, B. E. and Starz-Gaiano, M. (2015). Tissue landscape alters adjacent cell fates during *Drosophila* egg development. *Nat. Commun.* **6**, 7356. doi:10.1038/ncomms8356
- Martinsen, A., Schakman, O., Yerna, X., Dessy, C. and Morel, N. (2014). Myosin light chain kinase controls voltage-dependent calcium channels in vascular smooth muscle. *Pflugers Arch.* **466**, 1377-1389. doi:10.1007/s00424-013-1380-3
- McCray, P. B. Jr. (1993). Spontaneous contractility of human fetal airway smooth muscle. *Am. J. Respir. Cell Mol. Biol.* **8**, 573-580. doi:10.1165/ajrcmb.8.5.573
- McCulley, D., Wienhold, M. and Sun, X. (2015). The pulmonary mesenchyme directs lung development. *Curr. Opin. Genet. Dev.* **32**, 98-105. doi:10.1016/j.gde.2015.01.011
- Menshkykau, D., Kraemer, C. and Iber, D. (2012). Branch mode selection during early lung development. *PLoS Comput. Biol.* **8**, e1002377. doi:10.1371/journal.pcbi.1002377
- Metzger, R. J., Klein, O. D., Martin, G. R. and Krasnow, M. A. (2008). The branching programme of mouse lung development. *Nature* **453**, 745-750. doi:10.1038/nature07005
- Miller, L.-A. D., Wert, S. E., Clark, J. C., Xu, Y., Perl, A.-K. T. and Whitsett, J. A. (2004). Role of Sonic hedgehog in patterning of tracheal-bronchial cartilage and the peripheral lung. *Dev. Dyn.* **231**, 57-71. doi:10.1002/dvdy.20105
- Min, H., Danilenko, D. M., Scully, S. A., Bolon, B., Ring, B. D., Tarpley, J. E., DeRose, M. and Simonet, W. S. (1998). Fgf-10 is required for both limb and lung development and exhibits striking functional similarity to *Drosophila* branchless. *Genes Dev.* **12**, 3156-3161. doi:10.1101/gad.12.20.3156
- Miura, T. and Shiota, K. (2000). Time-lapse observation of branching morphogenesis of the lung bud epithelium in mesenchyme-free culture and its relationship with the localization of actin filaments. *Int. J. Dev. Biol.* **44**, 899-902.
- Mohammadi, M., McMahon, G., Sun, L., Tang, C., Hirth, P., Yeh, B. K., Hubbard, S. R. and Schlessinger, J. (1997). Structures of the tyrosine kinase domain of fibroblast growth factor receptor in complex with inhibitors. *Science* **276**, 955-960. doi:10.1126/science.276.5314.955
- Moiseenko, A., Kheirollahi, V., Chao, C.-M., Ahmadvand, N., Quantius, J., Wilhelm, J., Herold, S., Ahlbrecht, K., Morty, R. E., Rizvanov, A. A. et al. (2017). Origin and characterization of alpha smooth muscle actin-positive cells during murine lung development. *Stem Cells* **35**, 1566-1578. doi:10.1002/stem.2615
- Morrissey, E. E. and Hogan, B. L. M. (2010). Preparing for the first breath: genetic and cellular mechanisms in lung development. *Dev. Cell* **18**, 8-23. doi:10.1016/j.devcel.2009.12.010
- Nelson, C. M., Gleghorn, J. P., Pang, M.-F., Jaslove, J. M., Goodwin, K., Varner, V. D., Miller, E., Radisky, D. C. and Stone, H. A. (2017). Microfluidic chest cavities reveal that transmural pressure controls the rate of lung development. *Development* **144**, 4328-4335. doi:10.1242/dev.154823
- Neumann, N. M., Perrone, M. C., Veldhuis, J. H., Huebner, R. J., Zhan, H., Devreotes, P. N., Brodland, G. W. and Ewald, A. J. (2018). Coordination of receptor tyrosine kinase signaling and interfacial tension dynamics drives radial intercalation and tube elongation. *Dev. Cell* **45**, 67-82.e66. doi:10.1016/j.devcel.2018.03.011
- Nogawa, H., Morita, K. and Cardoso, W. V. (1998). Bud formation precedes the appearance of differential cell proliferation during branching morphogenesis of mouse lung epithelium in vitro. *Dev. Dyn.* **213**, 228-235. doi:10.1002/(SICI)1097-0177(199810)213:2<228::AID-AJA8>3.0.CO;2-I
- Pepicelli, C. V., Lewis, P. M. and McMahon, A. P. (1998). Sonic hedgehog regulates branching morphogenesis in the mammalian lung. *Curr. Biol.* **8**, 1083-1086. doi:10.1016/S0960-9822(98)70446-4
- Preibisch, S., Saalfeld, S. and Tomancak, P. (2009). Globally optimal stitching of tiled 3D microscopic image acquisitions. *Bioinformatics* **25**, 1463-1465. doi:10.1093/bioinformatics/btp184
- Radzikinas, K., Aven, L., Jiang, Z., Tran, T., Paez-Cortez, J., Boppidi, K., Lu, J., Fine, A. and Ai, X. (2011). A Shh/miR-206/BDNF cascade coordinates innervation and formation of airway smooth muscle. *J. Neurosci.* **31**, 15407-15415. doi:10.1523/JNEUROSCI.2745-11.2011
- Ramasamy, S. K., Mailloux, A. A., Gupte, V. V., Mata, F., Sala, F. G., Veltmaat, J. M., Del Moral, P. M., De Langhe, S., Parsa, S., Kelly, L. K. et al. (2007). Fgf10 dosage is critical for the amplification of epithelial cell progenitors and for the formation of multiple mesenchymal lineages during lung development. *Dev. Biol.* **307**, 237-247. doi:10.1016/j.ydbio.2007.04.033
- Roman, J. (1995). Effects of calcium channel blockade on mammalian lung branching morphogenesis. *Exp. Lung Res.* **21**, 489-502. doi:10.3109/01902149509031754
- Schnatwinkel, C. and Niswander, L. (2013). Multiparametric image analysis of lung-branching morphogenesis. *Dev. Dyn.* **242**, 622-637. doi:10.1002/dvdy.23961
- Shyer, A. E., Tallinen, T., Nerurkar, N. L., Wei, Z., Gil, E. S., Kaplan, D. L., Tabin, C. J. and Mahadevan, L. (2013). Villification: how the gut gets its villi. *Science* **342**, 212-218. doi:10.1126/science.1238842
- Shyer, A. E., Huyck, T. R., Lee, C. H., Mahadevan, L. and Tabin, C. J. (2015). Bending gradients: how the intestinal stem cell gets its home. *Cell* **161**, 569-580. doi:10.1016/j.cell.2015.03.041
- Spurlin, J. W., Siedlik, M. J., Nerger, B.-A., Pang, M.-F., Jayaraman, S., Zhang, R. and Nelson, C. M. (2019). Mesenchymal proteases and tissue fluidity remodel the extracellular matrix during airway epithelial branching in the embryonic avian lung. *Development* **146**, dev175257. doi:10.1242/dev.175257
- Swarr, D. T. and Morrissey, E. E. (2015). Lung endoderm morphogenesis: gasping for form and function. *Annu. Rev. Cell Dev. Biol.* **31**, 553-573. doi:10.1146/annurev-cellbio-100814-125249
- Tallinen, T., Chung, J. Y., Biggins, J. S. and Mahadevan, L. (2014). Gyrfication from constrained cortical expansion. *Proc. Natl. Acad. Sci. USA* **111**, 12667-12672. doi:10.1073/pnas.1406015111
- Tallinen, T., Chung, J. Y., Rousseau, F., Girard, N., Lefèvre, J. and Mahadevan, L. (2016). On the growth and form of cortical convolutions. *Nat. Phys.* **12**, 588-593. doi:10.1038/nphys3632
- Tzou, D., W. Spurlin, J., Ill, Pavlovich, A. L., Stewart, C. R., Gleghorn, J. P. and Nelson, C. M. (2016). Morphogenesis and morphometric scaling of lung airway development follows phylogeny in chicken, quail, and duck embryos. *Evodevo* **7**, 12. doi:10.1186/s13227-016-0049-3
- Varner, V. D. and Nelson, C. M. (2014). Cellular and physical mechanisms of branching morphogenesis. *Development* **141**, 2750-2759. doi:10.1242/dev.104794
- Varner, V. D., Gleghorn, J. P., Miller, E., Radisky, D. C. and Nelson, C. M. (2015). Mechanically patterning the embryonic airway epithelium. *Proc. Natl. Acad. Sci. USA* **112**, 9230-9235. doi:10.1073/pnas.1504102112
- Volckaert, T., Campbell, A., Dill, E., Li, C., Minoo, P. and De Langhe, S. (2013). Localized Fgf10 expression is not required for lung branching morphogenesis but prevents differentiation of epithelial progenitors. *Development* **140**, 3731-3742. doi:10.1242/dev.096560
- Wang, S., Sekiguchi, R., Daley, W. P. and Yamada, K. M. (2017). Patterned cell and matrix dynamics in branching morphogenesis. *J. Cell Biol.* **216**, 559-570. doi:10.1083/jcb.201610048
- Weaver, M., Batts, L. and Hogan, B. L. M. (2003). Tissue interactions pattern the mesenchyme of the embryonic mouse lung. *Dev. Biol.* **258**, 169-184. doi:10.1016/S0012-1606(03)00117-9
- Yang, Y., Beqaj, S., Kemp, P., Ariel, I. and Schuger, L. (2000). Stretch-induced alternative splicing of serum response factor promotes bronchial myogenesis and is defective in lung hypoplasia. *J. Clin. Invest.* **106**, 1321-1330. doi:10.1172/JCI8893
- Yi, L., Domyan, E. T., Lewandoski, M. and Sun, X. (2009). Fibroblast growth factor 9 signaling inhibits airway smooth muscle differentiation in mouse lung. *Dev. Dyn.* **238**, 123-137. doi:10.1002/dvdy.21831
- Zhao, X.-H., Laschinger, C., Arora, P., Szaszi, K., Kapus, A. and McCulloch, C. A. (2007). Force activates smooth muscle alpha-actin promoter activity through the Rho signaling pathway. *J. Cell Sci.* **120**, 1801-1809. doi:10.1242/jcs.001586

Supplementary Figure 1

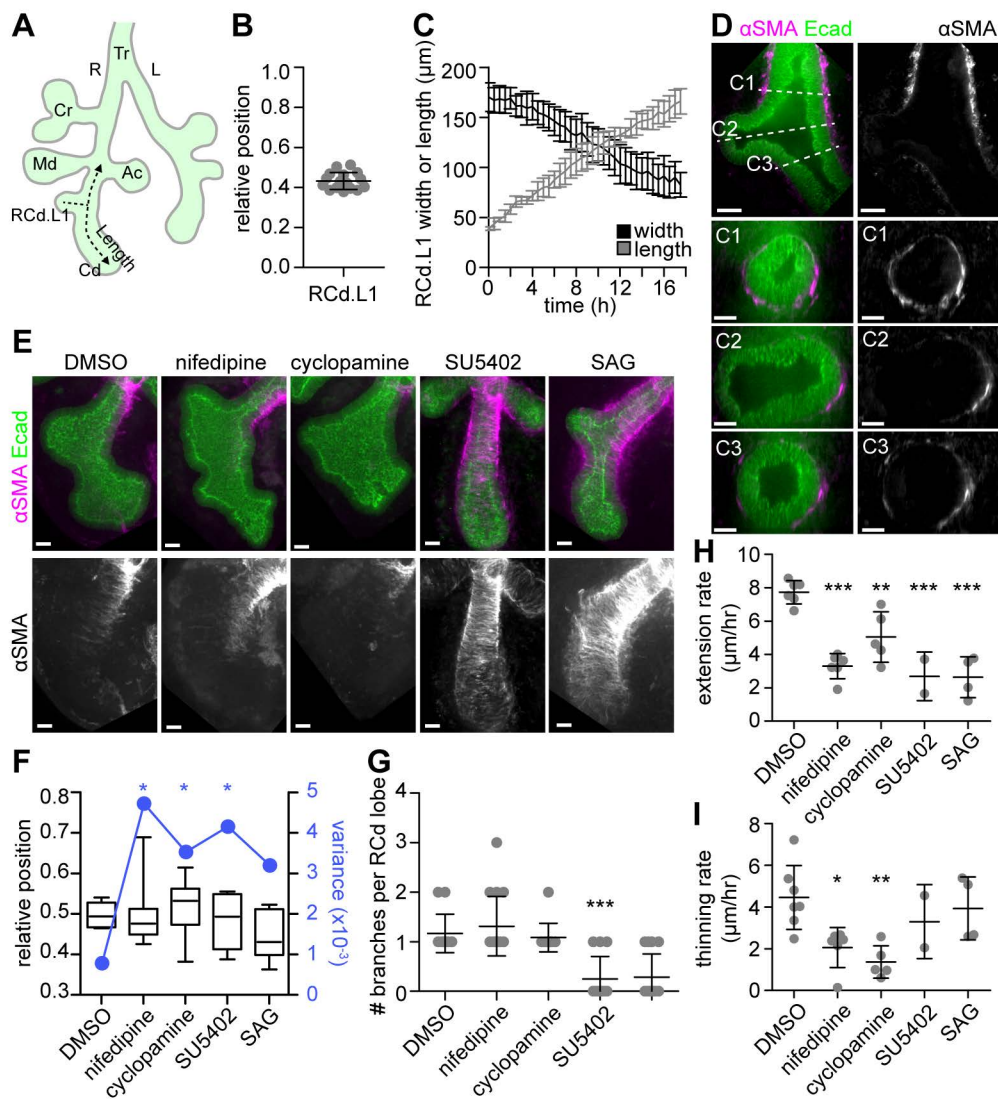


Figure S1 – related to Figures 1-3. Smooth muscle influences domain branch formation in the right caudal lobe. (A) Schematic of *E12* mouse lung showing the position of

domain branch RCd.L1 in the right caudal (RCd) lobe. (B) Relative position of RCd.L1 in *E12* lungs measured as distance from proximal end of RCd divided by length of RCd (n=16). Error bars indicate SD.

(C) Width and length of RCd.L1 over the course of 24 hr time-lapse imaging (n=5). Error bars indicate SD. (D) Single z-slices and reconstructed cross-sections of the RCd

lobe of an *E12* lung immunostained for Ecad and α SMA. Cross-sections are from locations C1-C3 indicated in top left image. (E) Z-projections of the RCd lobe of lungs isolated at *E11.5* and

then immunostained for Ecad and α SMA after treatment with either DMSO, nifedipine (10 μ M), cyclopamine (1 μ M), SU5402 (5 μ M), or SAG (0.5 μ g/ml) for 24 hr. (F) Relative position of

domain branch RCd.L1 and variance of position for each treatment (n=7-14). Whiskers show min and max values. Each group was compared using Bartlett's test for unequal variances. (G)

Number of branching or buckling events occurring over 24 hr time-lapse imaging in the RCd lobe of lungs for each treatment (n=9-18). Rate of change of domain branch RCd.L1 (H) length

and (I) width during 24 hr time-lapse imaging of treated lungs (n=4-7). Scale bars show 25 μ m.

*** indicates $p < 0.0001$, ** $p < 0.001$, * $p < 0.05$.

Supplementary Figure 2

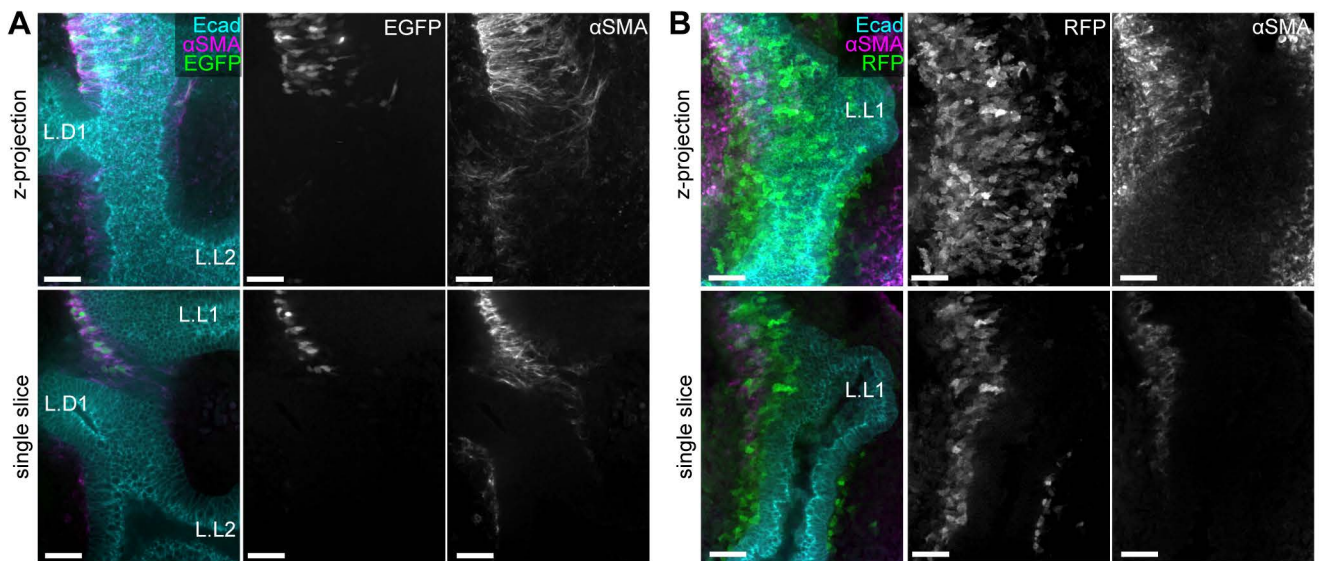


Figure S2 – related to Figure 1. Patterns of expression of smooth muscle markers. (A) Z-projections (top) and single slices (bottom) of lungs from mice expressing EGFP under the Myh11 promoter and immunostained for Ecad, α SMA, and EGFP. **(B)** Z-projections (top) and single slices (bottom) of lungs from mice expressing RFP under the α SMA promoter and immunostained for Ecad, α SMA, and RFP. Scale bars show 25 μ m.

Supplementary Figure 3

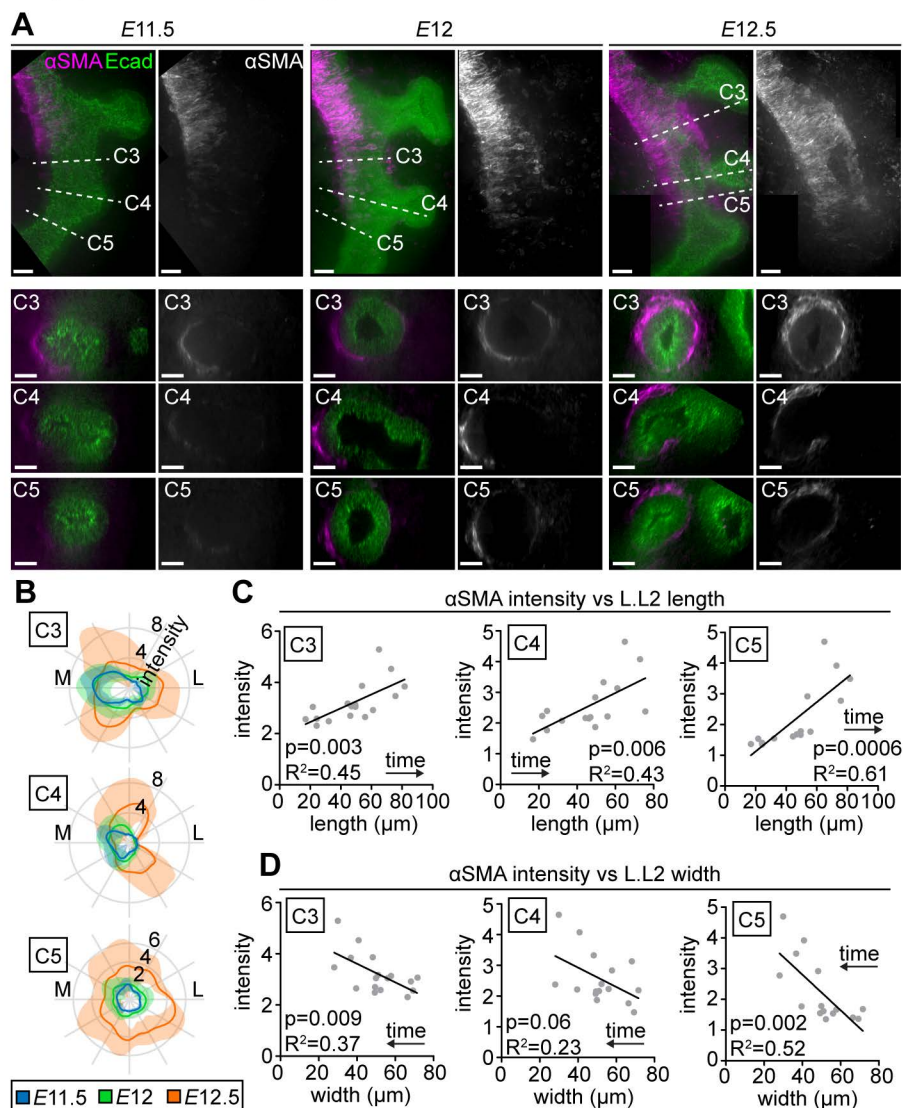


Figure S3 – related to Figure 1. Smooth muscle wrapping around the airway increases as domain branches elongate and thin. (A) Representative z-projections and reconstructed cross-sections of the left lobe of lungs immunostained for Ecad and α SMA at E11.5, E12, and E12.5. Scale bars show 25 μ m. **(B)** Polar plots showing mean α SMA intensity relative to background intensity around airway at C3-C5 for each group (n=4-9). Dark lines show mean and shaded regions show SD. Mean smooth muscle intensity around the airway versus **(C)** length or **(D)** width at the level of C3, C4, and C5 (n=15-17). Results of linear regression including p-value and R^2 values are indicated on each plot.

Supplementary Figure 4

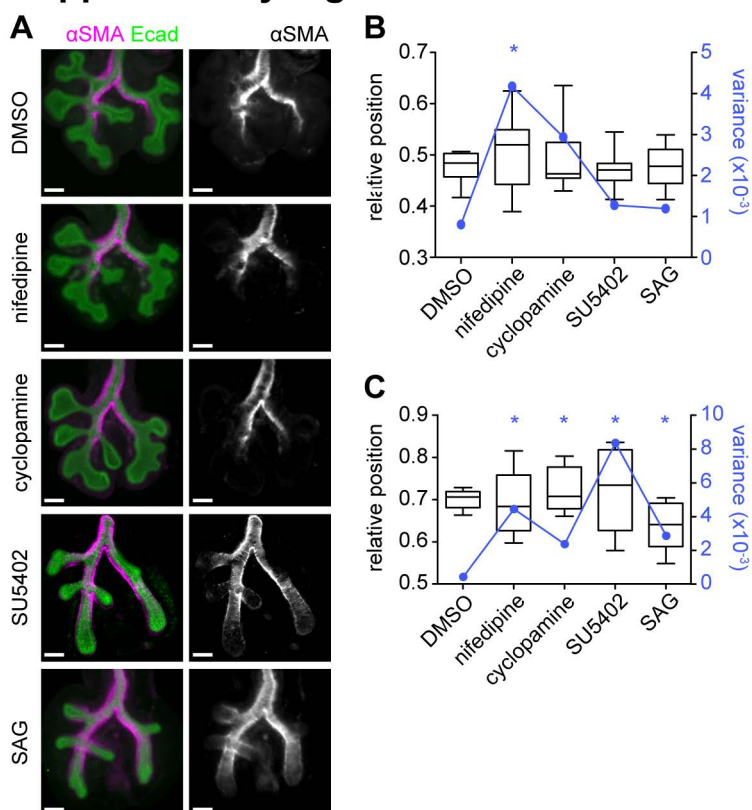
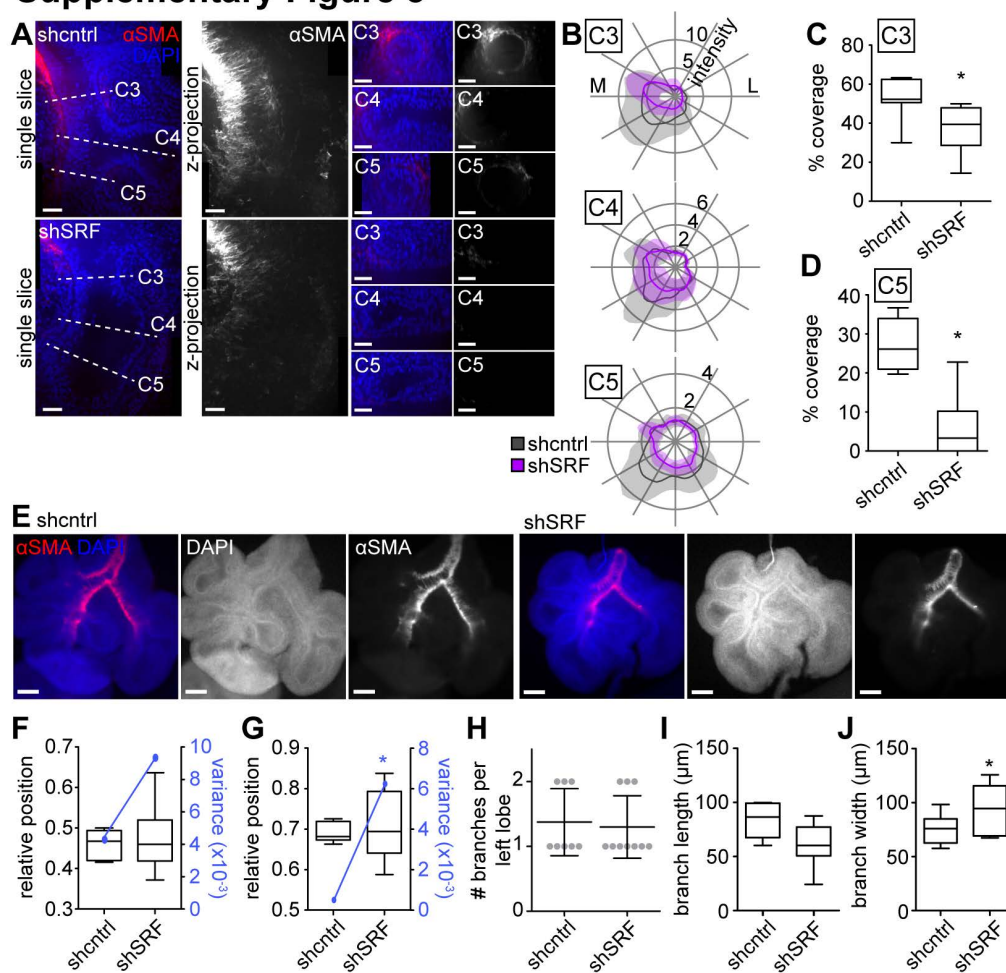


Figure S4 – related to Figure 2. Disruptions to smooth muscle differentiation affect smooth muscle localization and domain branching of the airway epithelium. (A) Images of whole lungs immunostained for Ecad and α SMA after treatment with either DMSO, nifedipine (10 μ M), cyclopamine (1 μ M), SU5402 (5 μ M), or SAG (0.5 μ g/ml) for 24 hr. Scale bars show 100 μ m. Relative position of domain branch (B) L.L1 and (C) L.L2 and variance of position for each treatment (n=10-15). Whiskers show min and max values. Each group was compared using Bartlett's test for unequal variances. * indicates $p < 0.05$.

Supplementary Figure 5

**Figure S5 – related to Figure 2. Mesenchyme-specific disruptions to smooth muscle****differentiation impair epithelial branching.** (A) Single confocal slices, z-projections, and

reconstructed cross-sections of the left lobe of lungs isolated at *E11.5* and then immunostained for αSMA and DAPI after transduction for 24 hr with either control (shcntrl) or shSRF adenoviruses. Cross-sections are from locations C3-C5 indicated in the left-most image. Scale bars show 25 μm .

(B) Polar plots showing mean total αSMA intensity relative to background intensity at C3, C4, and C5 ($n=6-9$).

(C-D) Quantification of αSMA coverage around the airway at C3 and C5 ($n=6-9$).

(E) Images of whole lungs immunostained for αSMA and DAPI after transduction with either control (shcntrl) or shSRF adenovirus for 24 hr. Scale bars show 100 μm .

Relative position of domain branch (F) L.L1 and (G) L.L2 and variance of position for each treatment ($n=4-16$). Whiskers show min and max values. Each group was compared using Bartlett's test for unequal variances.

(H) Number of domain branches that form in the left lobe after 24 hr culture. Domain branch L.L2 (I) length and (J) width after 24 hr

culture ($n=7-8$). * indicates $p<0.05$.

Supplementary Figure 6

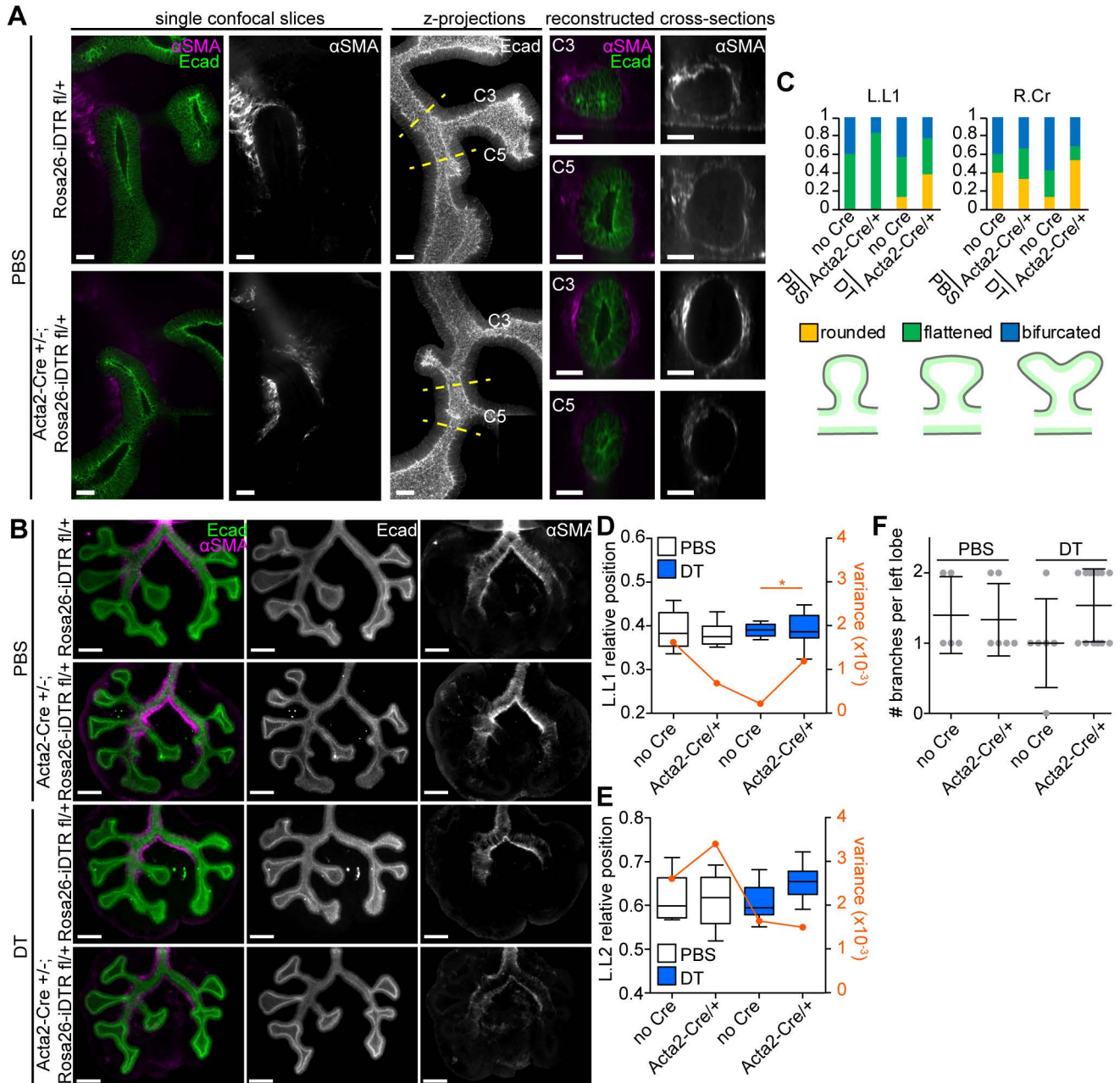


Figure S6 – related to Figure 4. Genetic ablation of smooth muscle cells using Acta2-Cre

impairs domain branching. (A) Single confocal slices, z-projections, and reconstructed cross-sections of the left lobe of Rosa26-iDTR fl/+ and Acta2-Cre/+; Rosa26-iDTR fl/+ lungs isolated at E11.5 and then immunostained for α SMA and Ecad after treatment for 24 hr with PBS. Cross-sections are from locations C3 and C5 indicated in the middle image. Scale bars show 25 μ m. (B) Images of whole lungs isolated from Rosa26-iDTR fl/+ and Acta2-Cre/+; Rosa26-iDTR fl/+ embryos and immunostained for Ecad and α SMA after treatment with either PBS or 0.2 ng/ μ l of DT. Scale bars show 100 μ m. (C) Fraction of cultured lungs with branch L.L1 and right cranial lobe (R.Cr) at each of stage of epithelial bifurcation, as indicated by the schematic below the legend. Relative position of domain branch (D) L.L1 and (E) L.L2 and variance of position for each treatment (n=5-13). Each group was compared using Bartlett's test for unequal variances. Whiskers show min and max values. (F) Number of domain branches that form in the left lobe after 24 hr culture. * indicates $p < 0.05$.

Supplementary Figure 7

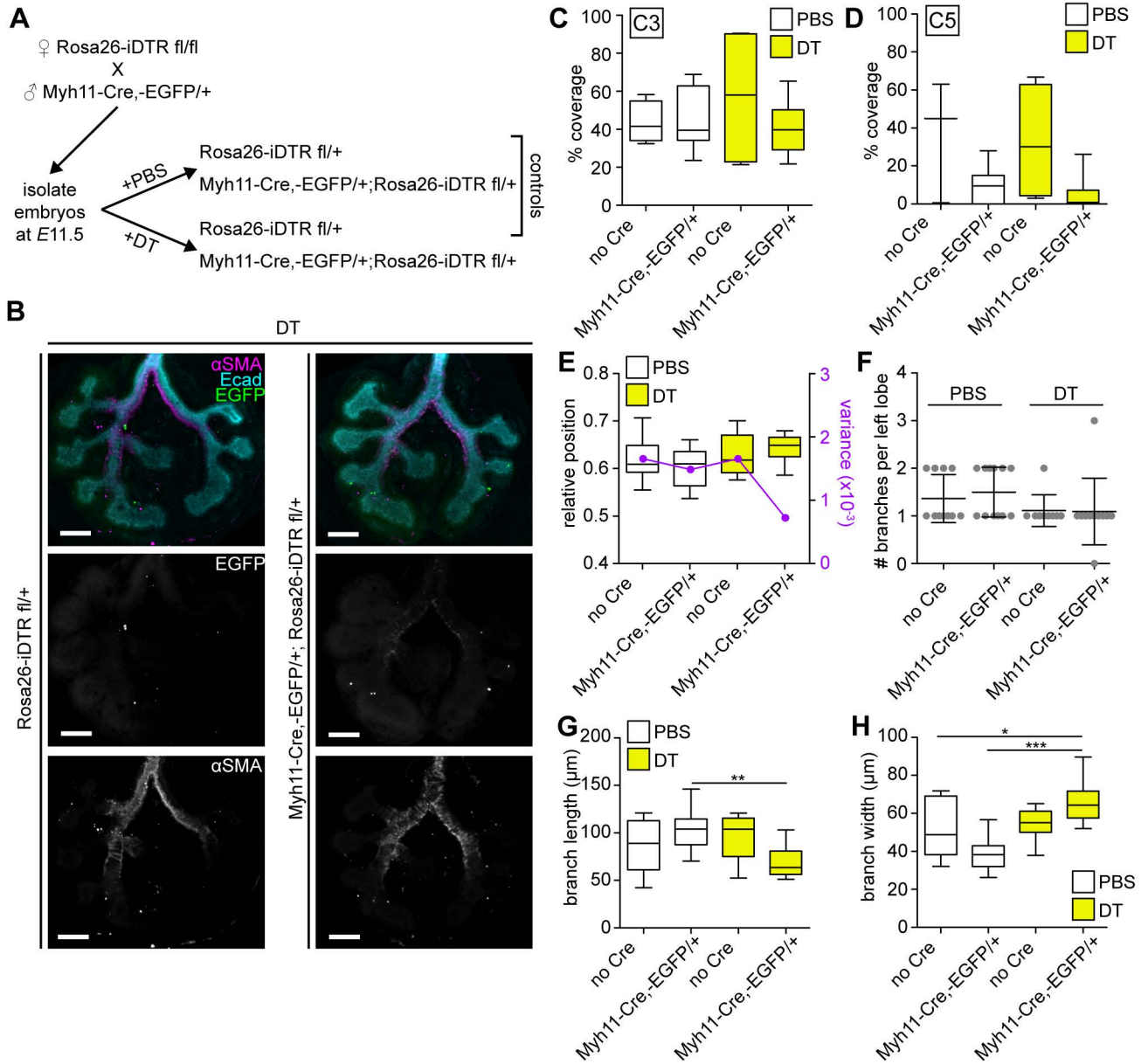


Figure S7 – related to Figure 4. Targeting mature smooth muscle cells using Myh11-Cre,-EGFP has no effect on smooth muscle coverage or domain branching. (A) Experimental scheme: Rosa26-iDTR fl/fl females are mated with Myh11-Cre,-EGFP/+ males. Embryos are isolated at E11.5 for ex vivo lung culture. Embryos of both possible genotypes are treated with either PBS or DT (0.5 ng/mL) for 24 hours. (B) Images of whole lungs isolated from Rosa26-iDTR fl/+ and Myh11-Cre,-EGFP/+;Rosa26-iDTR fl/+ embryos and immunostained for Ecad, EGFP, and α SMA after treatment with either PBS or 0.5 ng/ μ l of DT. Scale bars show 100 μ m. (C-D) Quantification of α SMA coverage around the airway proximal to L.L2 (C3) and distal to L.L2 (C5) (n=3-7). (E) Relative position of domain branch L.L2 and variance of position for each treatment (n=9-12). (F) Number of domain branches that form in the left lobe after 24 hr culture. (G) Length and (H) width of domain branch L.L2 after 24 hr culture (n=9-12). All genotypes indicated on plots include Rosa26-iDTR fl/+. Whiskers show min and max values. * indicates $p < 0.05$, ** $p < 0.001$, *** $p < 0.0001$.

Supplementary Figure 8

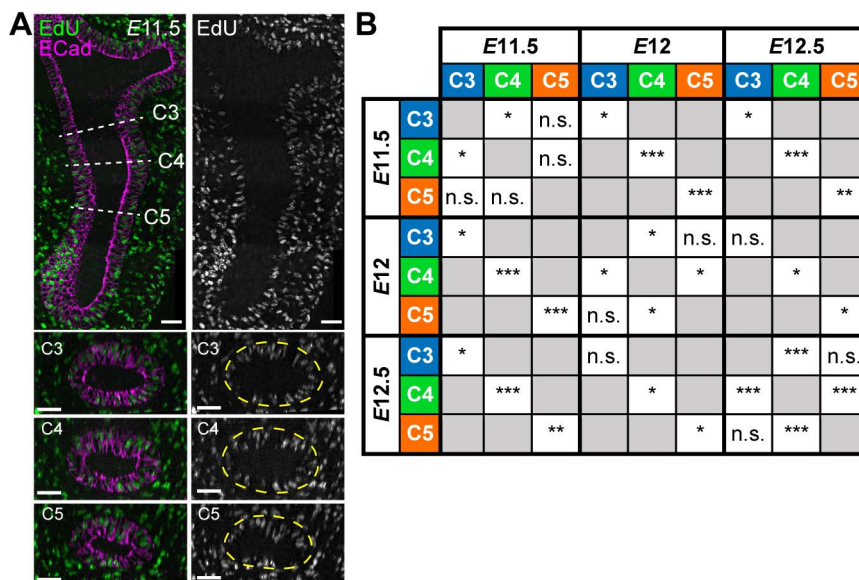


Figure S8 – related to Figure 5. Patterned epithelial proliferation in the distal left lobe. (A) Z-projections and reconstructed cross-sections of the left lobe of *E11.5* lungs after 30 min EdU pulse and immunostaining for Ecad. Cross-sections are from locations C3-C5 indicated in the left-most image. Scale bars show 25 μ m. **(B)** Statistical significance based on two-sided Kolmogorov-Smirnov test for comparisons between the angular distributions of EdU⁺ cells at cross-sections C3-C5 measured from lungs at *E11.5*, *E12*, and *E12.5* (from Figure 5B). *** indicates $p < 0.0001$, ** $p < 0.001$, * $p < 0.05$.

Supplementary Figure 9

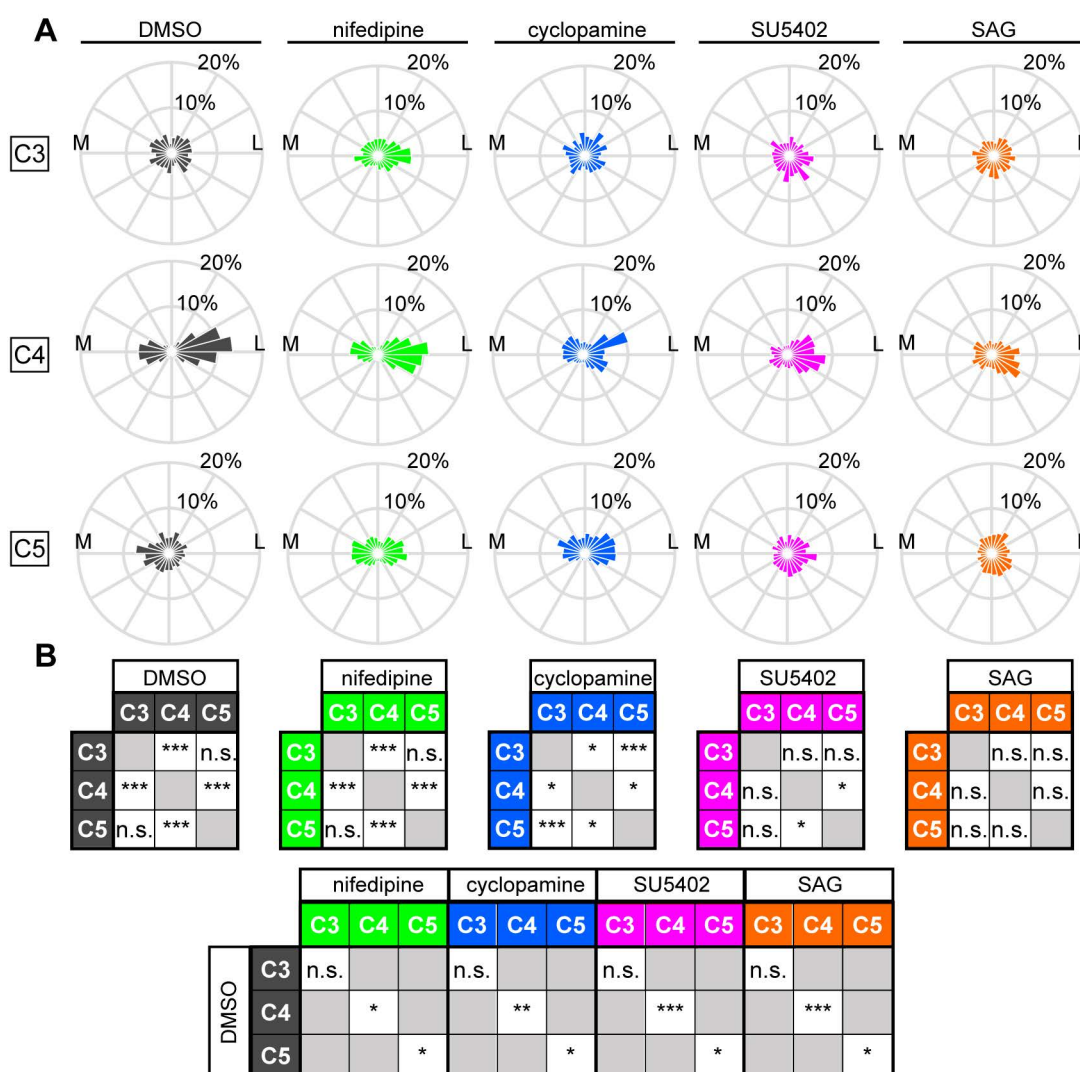


Figure S9 – related to Figure 5. Angular distributions of EdU⁺ cells in drug-treated lungs.

(A) Angular distributions of EdU⁺ cells with respect to the center of the primary bronchus at

cross-sections C3-C5 (n=6-14). (B) Statistical significance based on two-sided Kolmogorov-

Smirnov test for comparisons between relevant pairs of distributions. *** indicates $p < 0.0001$,

** $p < 0.001$, * $p < 0.05$.

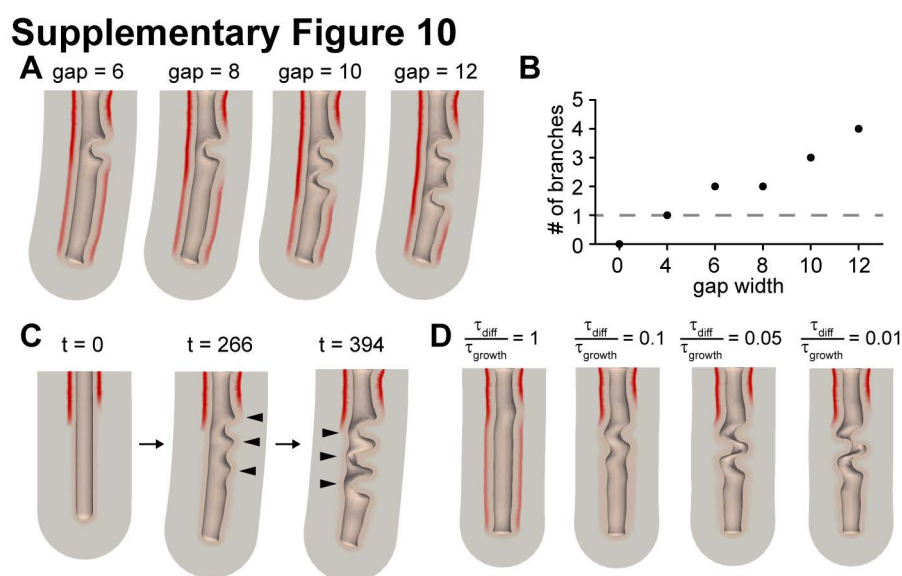
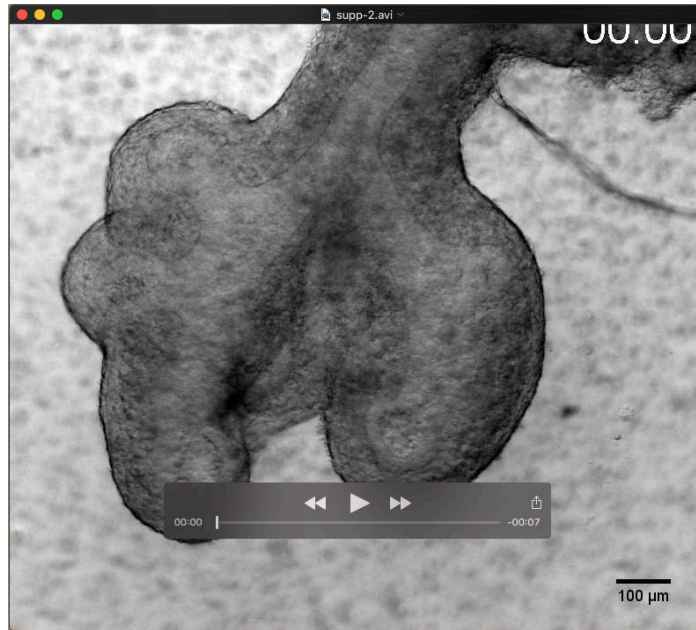
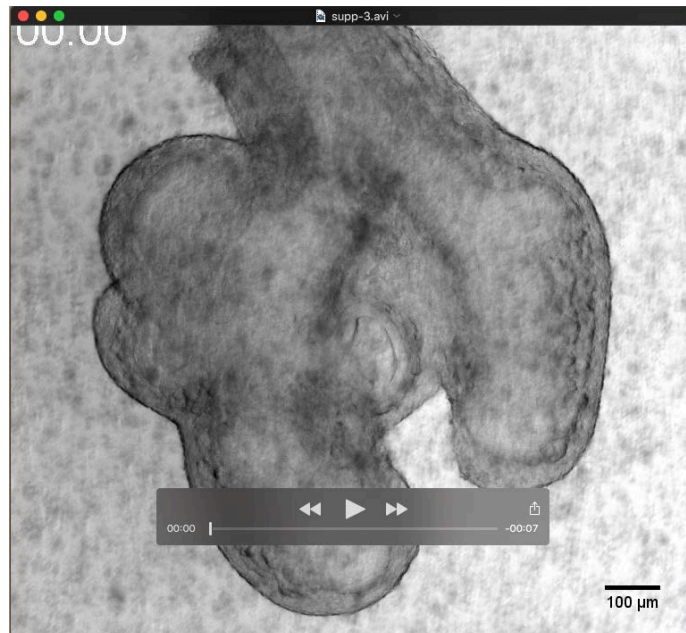


Figure S10 – related to Figure 7. The effects of gap size and relative growth on branching in a computational model of domain branching. (A) Snapshots at $t=4.5$ of simulations with gap sizes 6, 8, 10, and 12 times the inner radius of the simulated epithelial tube. In all cases, $\tau_{diff}/\tau_{growth} = 1$. **(B)** Quantification of the number of lateral branches in simulations with different gap sizes, expressed as 0 to 12 times the inner radius of the simulated epithelial tube. **(C)** Snapshots at $t=0$, $t=266$, and $t=394$ of a simulation with gap size 4 and $\tau_{diff}/\tau_{growth} = 0.01$. **(D)** Snapshots of simulations with the same growth rate on the lateral and medial sides at $t=4$ and with $\tau_{diff}/\tau_{growth} = 1, 0.1, 0.05$, and 0.01 .

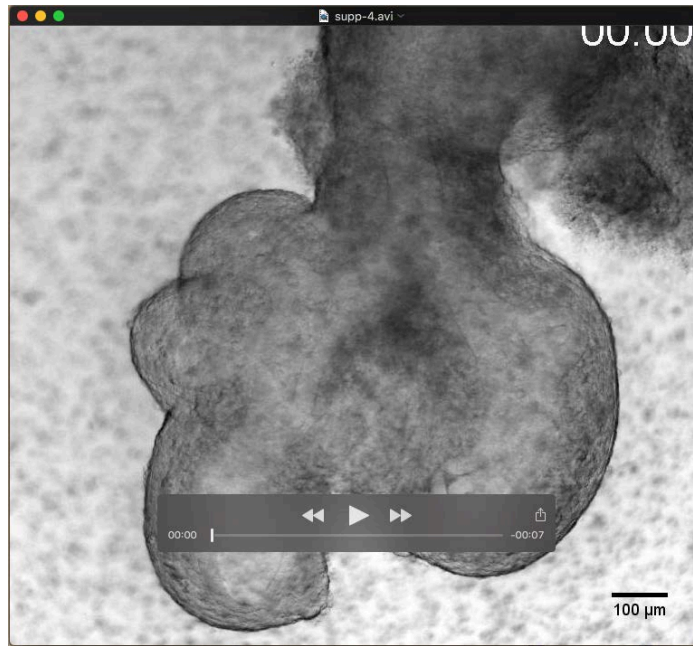
Supplementary Movies



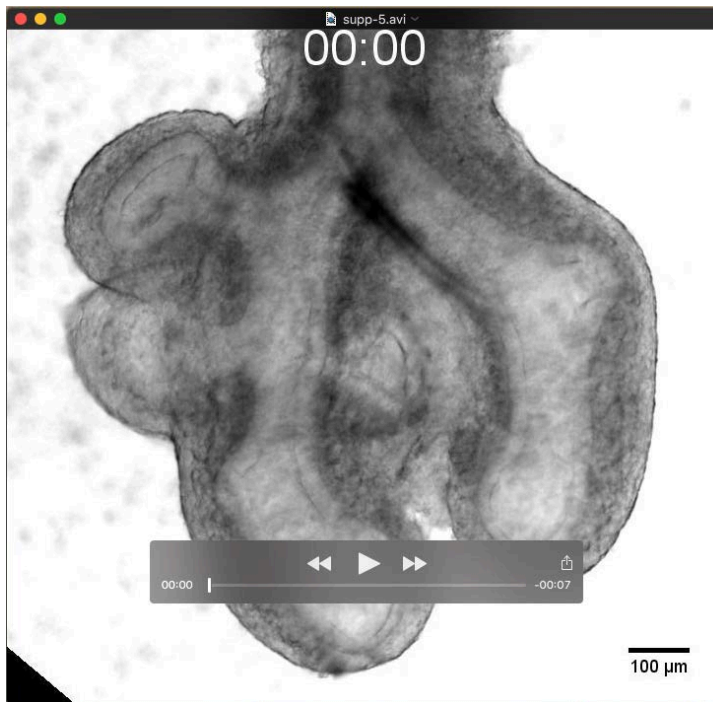
Movie 1. Time-lapse of lungs isolated at *E11.5* and cultured in the presence of DMSO for 24 hr.



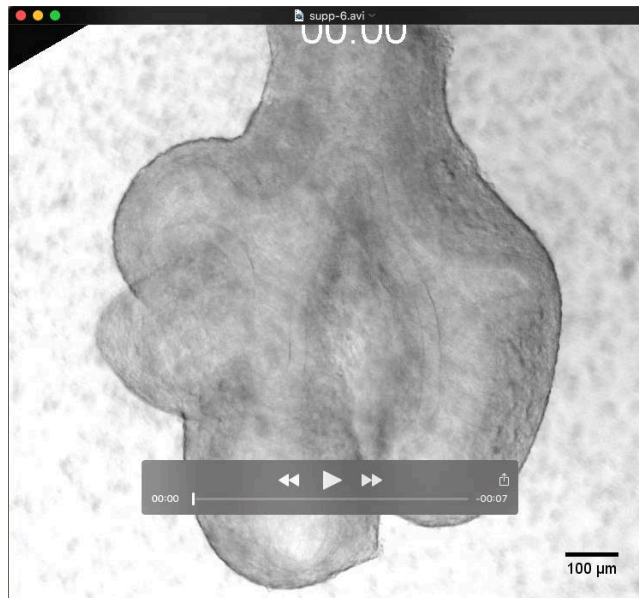
Movie 2. Time-lapse of lungs isolated at *E11.5* and cultured in the presence of nifedipine (10 μM) for 24 hr.



Movie 3. Time-lapse of lungs isolated at *E11.5* and cultured in the presence of cyclopamine (1 μM) for 24 hr.



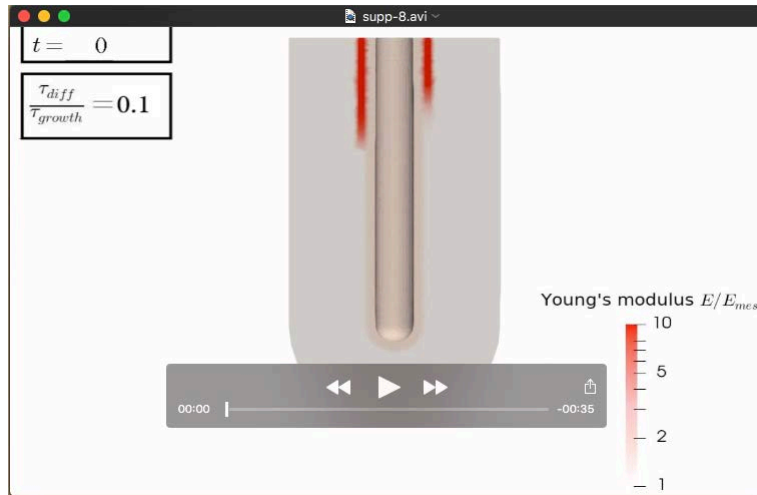
Movie 4. Time-lapse of lungs isolated at *E11.5* and cultured in the presence of SU5402 (10 μM) for 24 hr.



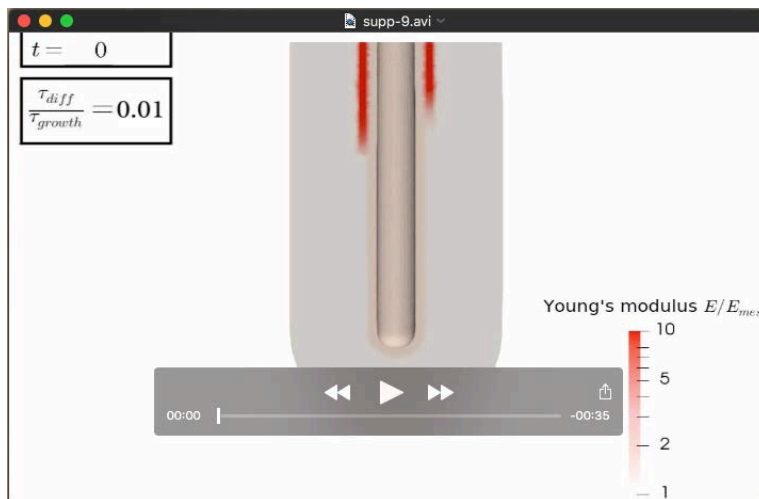
Movie 5. Time-lapse of lungs isolated at *E11.5* and cultured in the presence of SAG (0.5 μg/ml) for 24 hr.



Movie 6. Computational model of domain branching. Smooth muscle differentiation rate (τ_{diff}) is the same as the epithelial growth rate (τ_{growth}).



Movie 7. Computational model of domain branching. Smooth muscle differentiation rate (τ_{diff}) is 0.1 times that of growth rate (τ_{growth}).



Movie 8. Computational model of domain branching. Smooth muscle differentiation time (τ_{diff}) is 0.01 times that of growth rate (τ_{growth}).

Supplementary Methods: Computational Model

We developed a 3D computational model that takes into account epithelial growth, smooth muscle differentiation, large deformations, and non-linear elasticity, in order to uncouple the effects of patterned epithelial proliferation and smooth muscle differentiation on domain branching.

1. Geometry

As shown in **Fig. 7A**, the primary bronchus is modeled as a hollow cylindrical tube with a spherical cap at the bottom. The tube has length L with inner radius R_{in} and outer radius R_{out} .

2. Physical Properties

The tube is comprised of three different tissue compartments: the epithelium, the airway smooth muscle, and the undifferentiated mesenchyme, as depicted in **Fig. 7**. These tissues are denoted by the subscripts ep , sm and mes , respectively. In our simplified model, all tissues are modeled as purely elastic materials.

3. Mechanical Model

To model growing tissues, we adopted the method of (Rodriguez et al, 1994), where the total deformation from the reference state is decomposed into that due to growth and that due to elastic deformation. We assume that growth and smooth muscle differentiation are much slower than mechanical relaxation and hence the system is always in quasi-mechanical equilibrium, which is achieved by minimizing the total elastic energy as described below.

Suppose that the initial reference volume is Ω and we introduce a fixed Cartesian coordinate system with an orthonormal basis $\{\mathbf{e}_1, \mathbf{e}_2, \mathbf{e}_3\}$ and spatial coordinates given as X_1, X_2, X_3 , denoted as $\mathbf{X} = X_i \mathbf{e}_i$, where summation over repeated indices is implied. At some later time t , the system is deformed to a volume Ω_t and the Cartesian coordinates get mapped to a different vector field, denoted as $\mathbf{x} = \boldsymbol{\varphi}(\mathbf{X})$.

To account for large deformation, we follow the finite deformation theory (Ogden, 1997) and define the deformation gradient tensor as:

$$F_{ij} = \frac{\partial x_i}{\partial X_j}. \quad (1)$$

The total deformation gradient can be decomposed as $\mathbf{F} = \mathbf{F}^e \mathbf{F}^g$, where it is assumed that the growth induces an intermediate stress-free state with a deformation gradient \mathbf{F}^g (referred to as growth tensor from here on) and that there is an additional elastic deformation to the final deformed state due to the elastic deformation gradient \mathbf{F}^e (Rodriguez et al, 1994).

To account for large material deformation, we use a Neo-Hookean model and assume the following elastic energy storage density Ψ (Ogden, 1997):

$$\Psi(\mathbf{F}^e = \mathbf{F} \mathbf{F}^g{}^{-1}) = \frac{\mu}{2}(I_c^e - 3 - 2 \ln J^e) + \frac{\lambda}{2}(\ln J^e)^2, \quad (2)$$

where λ and μ are the Lamé constants that are related to the Young's modulus E and Poisson ratio ν as:

$$\mu = \frac{E}{2(1 + \nu)}, \quad \lambda = \frac{E\nu}{(1 - 2\nu)(1 + \nu)}.$$

$I_c^e = \text{tr}(\mathbf{C})$ is the trace of the right Cauchy-Green deformation tensor $\mathbf{C} = (\mathbf{F}^e)^T \mathbf{F}^e$, and $J^e =$

$\det(\mathbf{F}^e) > 0$ is the Jacobian of the elastic deformation gradient. Epithelium, airway smooth muscle, and undifferentiated mesenchyme are characterized with different material constants.

4. Growth Tensor

Deformation due to growth is uniquely determined by the growth tensor \mathbf{F}^g . For simplicity, we assume that the undifferentiated mesenchyme and smooth muscle are not proliferating, i.e.

$\mathbf{F}_{sm}^g = \mathbf{F}_{mes}^g = \mathbf{I}$. Based on our experimental observations, the epithelium is assumed to grow

only along the axial direction of the tube, such that $\mathbf{F}_{ep}^g = \begin{pmatrix} 1 & 0 & 0 \\ 0 & 1 & 0 \\ 0 & 0 & g \end{pmatrix}$, where g is the growth

component, the magnitude of which depends on the position along the epithelium. According to our experimental observations (**Fig. 5B**), epithelial proliferation is non-uniform along the angular direction θ and is increased on the lateral side ($\theta = 0$). To account for this, we model epithelial growth as $g = g_0 + (g_1 - g_0)(1 - \cos\theta)/2$, where growth on the lateral side ($\theta = 0$) is g_0 and growth on the medial side ($\theta = \pi$) is g_1 . The values of g_0 and g_1 increase linearly as the epithelium proliferates.

Patterned differentiation of smooth muscle from the surrounding undifferentiated mesenchyme is modeled as a gradual increase in the Young's modulus of the tissue from E_{mes} to E_{sm} :

$$E(t) = E_{sm} \phi(t) + E_{mes} [1 - \phi(t)], \quad (3)$$

where $\phi = 0$ marks the initiation of smooth muscle differentiation and $\phi = 1$ corresponds to full differentiation. Smooth muscle stiffness is assumed to increase linearly over time, such that

$$\phi(t) = \begin{cases} t/t_{diff}, & t \leq t_{diff} \\ 1, & t > t_{diff} \end{cases} \quad (4)$$

An important parameter is the relative speed of smooth muscle differentiation compared to the rate of proliferation of the epithelium (described in more detail below).

5. Boundary Conditions

The top of the system is fixed in the vertical direction, and we fix 3 more degrees of freedom to remove possible rigid body movements in the \mathbf{e}_1 - \mathbf{e}_2 plane. The outer surface of the tube is considered traction free. The inner surface is loaded with a positive normal pressure p , which is in the opposite direction of outer normal \mathbf{n} (in the deformed configuration). That is to say on the inner surface, the traction force \mathbf{t} can be written as:

$$\mathbf{t} = -p\mathbf{n}. \quad (5)$$

6. Finite Element Method

The finite element method (FEM) is a standard method in computational mechanics to numerically solve for the deformation field under given boundary conditions (Bathe, 1996). More specifically, the task is to calculate the displacement field $u_i = x_i - X_i$ that minimizes the total potential energy Π , i.e. $\mathbf{u} = \arg \min_{\mathbf{u} \in V_u} \Pi$ for a prescribed growth profile with deformation gradient \mathbf{F}^g . Here V_u is the function space that satisfies boundary conditions on \mathbf{u} and the total potential energy can be written as (Dervaux and Ben Amar, 2011; Ahrens et al, 2005):

$$\Pi = \int_{\Omega} J^g \Psi(\mathbf{F}^e) d\mathbf{X} - \int_{\partial\Omega_t^{in}} \mathbf{t} \cdot \mathbf{u} ds \quad (6)$$

where $J^g = \det(\mathbf{F}^g) > 0$ is the Jacobian of the deformation gradient \mathbf{F}^g due to growth. ds and $\partial\Omega_t^{in}$ are the infinitesimal surface elements and the inner surface boundary in the deformed configuration respectively. Minimizing the above potential energy is to solve the following equation:

$$0 = \delta\Pi = \int_{\Omega} \left[J^g \frac{\partial\Psi(\mathbf{F}^e)}{\partial\mathbf{u}} \right] \delta\mathbf{u} d\mathbf{X} - \int_{\partial\Omega_t^{in}} \mathbf{t} \cdot \delta\mathbf{u} ds, \quad (7a)$$

$$= \int_{\Omega} \left[J^g \frac{\partial\Psi(\mathbf{F}^e)}{\partial\mathbf{u}} \right] \delta\mathbf{u} d\mathbf{X} + \int_{\partial\Omega^{in}} p(J\mathbf{F}^{-T}\mathbf{N}) \cdot \delta\mathbf{u} dS, \quad (7b)$$

where dS and $\partial\Omega^{in}$ are the infinitesimal surface elements and the inner surface boundary in the reference configuration, respectively. $J = \det(\mathbf{F}) > 0$ is the Jacobian of the total deformation tensor \mathbf{F} . The virtual work due to pressure p in the second Eq. (7b) is translated to the undeformed reference configuration by using the Nanson's formula, where \mathbf{N} is the outer normal in the reference configuration (Ogden, 1997).

To numerically solve the above minimization problem, the domain Ω is discretized using first-order tetrahedral elements that were generated with the help of an open source software Gmsh (Geuzaine and Remacle, 2009). Then, the nonlinear minimization problem is implemented in the open-source computing platform FEniCS (Alnæs et al., 2015). Generally, we use the Newton-Raphson algorithm (Kendall, 1989) to find the minimum of the non-linear problem. However, the Newton's method fails to converge near the wrinkling/branching instability because the energy landscape becomes saddle-shaped. Whenever the Newton's method failed to converge, we resorted to the more robust dynamic relaxation method (Underwood, 1983) to find the energy minimum. Accuracy of the obtained results were tested against mesh refinements.

Growth is increased in a linear form, i.e. $g_0 = 1 + \Delta g_0 t$ and $g_1 = 1 + \Delta g_1 t$. For each time step, we computed the equilibrium configuration \mathbf{x} by solving Eq. (7b). The results were visualized using Paraview software (Ahrens et al., 2005).

The geometrical parameters were chosen based on experimentally measured values and are expressed relative to the inner radius R_{in} of the tube. The thickness of the epithelium was $h_{ep}/R_{in} = 0.7$, the thickness of airway smooth muscle $h_{sm}/R_{in} = 0.3$, and the thickness of undifferentiated mesenchyme $h_{mes}/R_{in} = 5.0$. The length of the tube was set to $L/R_{in} = 18$ and the gap within differentiated smooth muscle was set to $L_{gap}/R_{in} = 4.0$. The Young's moduli were set to: $E_{sm}/E_{mes} = 10.0$, $E_{ep}/E_{mes} = 1.5$ and the pressure inside tube was $p/E_{mes} = 0.10$. The Poisson's ratios of all three tissues were taken to be 0.40.

For growth parameters, we used values $\Delta g_0 = 3\Delta g_1 = 0.01$ per simulation step, where the total number of time steps is $t_{growth} = 700$. The relative duration of smooth muscle differentiation (t_{diff}) was varied in different simulations in the range $\frac{t_{diff}}{t_{growth}} \in (1, 100)$. For ease of discussion, we report the results in terms of relative differentiation rate, where rate $\tau_{diff} = 1/t_{diff}$. Fast (slow) smooth muscle differentiation corresponds to large (small) values of $\frac{t_{diff}}{t_{growth}}$.

References

Ahrens, J., Geveci, B., Law, C. (2005). ParaView: An End-User Tool for Large Data Visualization, Visualization Handbook (Elsevier).

Alnæs, M., Blechta, J., Hake, J., Johansson, A., Kehlet, B., Logg, A., Richardson, C., Ring, J., Rognes, M.E., and Wells, G.N. (2015). The FEniCS Project Version 1.5. Archive of Numerical Software 3.

Bathe, K.-J. (1996). Finite Element Procedures (Prentice Hall).

Dervaux, J., Ben Amar, M. (2011). Buckling condensation in constrained growth, Journal of the Mechanics and Physics of Solids, 59 (3), 538-560.

Geuzaine, C., and Remacle, J. F. (2009). Gmsh: A 3-D finite element mesh generator with built-in pre- and post-processing facilities. International Journal for Numerical Methods in Engineering 79, 1309–1331.

Kendall, E. A. (1989). An Introduction to Numerical Analysis (John Wiley & Sons).

Ogden, R.W. (1997). Non-linear Elastic Deformations (Courier Corporation).

Rodriguez, E.K., Hoger, A., and McCulloch, A.D. (1994). Stress-dependent finite growth in soft elastic tissues. Journal of Biomechanics 27, 455–467.

Underwood, P. (1983). Dynamic Relaxation. In Computational Methods for Transient Analysis, North-Holland: Amsterdam, pp. 245-265. Belytschko, T., Hughes TJR.